Control of bone formation by the serpentine receptor Frizzled-9

Joachim Albers,[1] Jochen Schulze,[1] F. Timo Beil,[1] Matthias Gebauer,[2] Anke Baranowsky,[1] Johannes Keller,[1] Robert P. Marshall,[1] Kristofer Wintges,[1] Felix W. Friedrich,[1] Matthias Priemel,[2] Arndt F. Schilling,[1] Johannes M. Rueger,[2] Kerstin Cornils,[3] Boris Fehse,[3] Thomas Streichert,[4] Guido Sauter,[5] Franz Jakob,[6] Karl L. Insogna,[7] Barbara Pober,[8] Klaus-Peter Knobeloch,[9] Uta Francke,[10] Michael Amling,[1] and Thorsten Schinke[1]

[1]Department of Osteology and Biomechanics, [2]Department of Trauma, Hand, and Reconstructive Surgery, [3]Department for Stem Cell Transplantation, [4]Institute of Clinical Chemistry, and [5]Department of Pathology, University Medical Center Hamburg-Eppendorf, 20246 Hamburg, Germany
[6]Orthopedic Department, University of Würzburg, 97074 Würzburg, Germany
[7]Department of Internal Medicine, Yale School of Medicine, New Haven, CT 06519
[8]Department of Pediatrics, Massachusetts General Hospital, Boston, MA 02114
[9]Department of Neuropathology, University Clinic Freiburg, Freiburg 79106, Germany
[10]Department of Genetics, Stanford University School of Medicine, Stanford, CA 94305

Although Wnt signaling in osteoblasts is of critical importance for the regulation of bone remodeling, it is not yet known which specific Wnt receptors of the Frizzled family are functionally relevant in this process. In this paper, we show that *Fzd9* is induced upon osteoblast differentiation and that *Fzd9*$^{-/-}$ mice display low bone mass caused by impaired bone formation. Our analysis of *Fzd9*$^{-/-}$ primary osteoblasts demonstrated defects in matrix mineralization in spite of normal expression of established differentiation markers. In contrast, we observed a reduced expression of chemokines and interferon-regulated genes in *Fzd9*$^{-/-}$ osteoblasts. We also identified the ubiquitin-like modifier Isg15 as one potential downstream mediator of Fzd9 in these cells. Importantly, our molecular analysis further revealed that canonical Wnt signaling is not impaired in the absence of Fzd9, thus explaining the absence of a bone resorption phenotype. Collectively, our results reveal a previously unknown function of Fzd9 in osteoblasts, a finding that may have therapeutic implications for bone loss disorders.

Introduction

Bone is constantly remodeled through the activities of bone-forming osteoblasts and bone-resorbing osteoclasts (Harada and Rodan, 2003; Teitelbaum and Ross, 2003). Because a relative increase of bone resorption over bone formation can result in osteoporosis, one of the most prevalent disorders in the aged population, it is important to understand the molecular mechanisms regulating the differentiation and activity of osteoblasts and osteoclasts (Sambrook and Cooper, 2006; Zaidi, 2007). Although there are already valuable therapeutic strategies to inhibit bone resorption in osteoporotic patients (Liberman, 2006; Cummings et al., 2009), it is especially required to identify additional molecular targets on osteoblasts because clinical observations have demonstrated that the risk of skeletal fractures is increased in patients with dysfunctional osteoclasts, whereas it is decreased in states of overactivated osteoblasts, as is the case in individuals with osteosclerosis (Rodan and Martin, 2000). In this regard, it was a major breakthrough when the transmembrane protein LRP5 had been identified as a regulator of bone formation in humans and a possible target for osteoanabolic therapy.

LRP5, together with LRP6, is the human orthologue of the *Drosophila melanogaster* protein arrow, a coreceptor for wingless, the fly homologue of mammalian Wnt ligands (Wehrli et al., 2000). Inactivating mutations of the human *LRP5* gene results in osteoporosis pseudoglioma syndrome, whereas activating mutations causes osteosclerosis (Gong et al., 2001; Boyden et al., 2002; Little et al., 2002). The key role of LRP5 in the regulation of bone mass in humans is further underscored

J. Albers and J. Schulze contributed equally to this paper.

Correspondence to Thorsten Schinke: schinke@uke.uni-hamburg.de

Abbreviations used in this paper: Fzd, Frizzled; µCT, microcomputed tomography; Opg, osteoprotegerin; qRT-PCR, quantitative RT-PCR; TRAP, tartrate-resistant acid phosphatase; WBS, Williams–Beuren syndrome.

The Rockefeller University Press $30.00
J. Cell Biol. Vol. 192 No. 6 1057–1072
www.jcb.org/cgi/doi/10.1083/jcb.201008012

by the findings of several investigators that demonstrated an association of single nucleotide polymorphisms within the *LRP5* gene with decreased bone mineral density and an increased risk of osteoporotic fractures (Grundberg et al., 2008; Richards et al., 2008; van Meurs et al., 2008). Based on this cumulative evidence, but also because of its transmembrane localization, LRP5 has been considered an excellent target molecule for osteoanabolic therapy. Moreover, because LRP5 has been suggested to act as a coreceptor for ligands of the Wnt family (Mao et al., 2001), it appeared reasonable to speculate that Wnt signaling in osteoblasts is physiologically involved in the control of bone formation.

One way to address this issue was the cell type–specific inactivation of β-catenin, whose stabilization and entry into the nucleus is the key step in the canonical Wnt signaling pathway (Wodarz and Nusse, 1998). Consistent with the expected requirement of this pathway for osteoblast differentiation, it has been demonstrated that an inactivation of β-catenin in mesenchymal progenitor cells causes an arrest of osteoblast differentiation and defects of skeletal development (Day et al., 2005, Hill et al., 2005; Hu et al., 2005). Unexpectedly however, when β-catenin was specifically inactivated in mature osteoblasts or in terminally differentiated osteocytes, a low bone mass phenotype was observed, which was not caused by decreased bone formation but by activated bone resorption (Glass et al., 2005; Holmen et al., 2005; Kramer et al., 2010). Because the opposite phenotype was observed upon osteoblast-specific activation of β-catenin, it is now commonly accepted that the canonical Wnt signaling pathway in osteoblasts primarily controls bone resorption, which is molecularly explained by an effect on the expression of *Tnfrsf11b*, the gene encoding the osteoclastogenesis inhibitor osteoprotegerin (Opg; Glass et al., 2005).

Because *Lrp5* deficiency in mice and humans specifically affects bone formation (Gong et al., 2001; Kato et al., 2002), these results further suggested that Lrp5 has no influence on canonical Wnt signaling in osteoblasts. This has been demonstrated by the finding that mice specifically lacking *Lrp5* in osteoblasts do not display a bone-remodeling phenotype, whereas a specific deletion of *Lrp5* in the duodenum causes decreased bone formation (Yadav et al., 2008). The molecular explanation for this indirect influence of Lrp5 on bone mass lies in the regulation of serotonin production in enterochromaffin cells, in which Lrp5 negatively regulates the expression of *Tph1*, the rate-limiting enzyme of peripheral serotonin synthesis. As a result, serotonin levels are increased in the absence of Lrp5, thereby causing low bone formation because gut-derived serotonin has a negative effect on osteoblast proliferation (Yadav et al., 2008). While increased circulating serotonin levels have also been observed in individuals with osteoporosis pseudoglioma syndrome, reduced levels were found in carriers of LRP5-activating mutations, thereby confirming that the mouse observations are also relevant in humans (Frost et al., 2010; Ramirez Rodriguez et al., 2010; Saarinen et al., 2010).

Although these results have demonstrated that Lrp5 controls bone mass through a different mechanism, there is still hallmark evidence for a direct influence of Wnt signaling in osteoblasts on bone remodeling. Despite the aforementioned role of β-catenin in the regulation of osteoclastogenesis, there is in vivo evidence for a negative regulation of bone formation by Wnt antagonists, such as Dkk1, Krm2, or Sfrp1 (Bodine et al., 2004; Li et al., 2006; Morvan et al., 2006; Schulze et al., 2010). Moreover, the findings that mice carrying a hypomorphic mutation of *Lrp6* display low bone mass and that polymorphisms of the human *LRP6* gene have an influence on bone mineral density provide further evidence for a critical role of Wnt signaling in the control of bone remodeling, independent of Lrp5 (Kubota et al., 2008; Sims et al., 2008). However, because both Lrp5 and Lrp6 only serve as coreceptors for the binding of Wnt ligands to receptors of the Frizzled (Fzd) family (Schulte and Bryja, 2007), it is surprising that there is yet no reported skeletal phenotype for a mouse model with impaired expression of one of the 10 known *Fzd* genes. In our opinion, it is of tremendous importance to fill this apparent gap in our understanding of Wnt signaling in bone cells because Fzd proteins belong to the family of serpentine receptors, which represent the major class of target proteins for currently available drugs (Wise et al., 2002; Overington et al., 2006). In this paper, we report that *Fzd9* is the only *Fzd* gene that is differentially expressed during the early stages of osteoblast differentiation and that mice lacking *Fzd9* display a cell-autonomous defect of bone formation.

Results

Fzd9 expression increases during early osteoblast differentiation

In an attempt to identify genes whose expression increases during the early stages of osteoblast differentiation, we performed a genome-wide expression analysis using GeneChip (Affymetrix) hybridization, thereby comparing primary osteoblasts derived from wild-type mice before the addition of ascorbate and β-glycerophosphate (day 0) and 5 d thereafter (day 5). By sorting all genes according to their signal log ratio between day 0 and day 5, we observed that the expression of *Fzd9* increased more than twofold, and the same was the case for well-established osteoblast differentiation markers, such as *Ibsp* (encoding bone sialoprotein), *Bglap* (encoding osteocalcin), and *Runx2* (Fig. 1 A). Because the expression of the other genes encoding Fzd receptors did not change between day 0 and day 5 of differentiation, these results led us to analyze the potential role of Fzd9 in bone remodeling.

Before doing so, we confirmed the results obtained by GeneChip hybridization in independently isolated osteoblast cultures. This was performed by quantitative RT-PCR (qRT-PCR; Fig. 1 B) and Western blotting (Fig. 1 C), in which we observed that the Fzd9 mRNA and protein levels increase during the initial stages of osteoblast differentiation and remain high until day 25 of culturing, in which the extracellular matrix is fully mineralized. We next analyzed the expression pattern of *Fzd9* in various tissues and cultured bone cells by RT-PCR, in which specific transcripts were readily detected in kidney, heart, eye, thyroid, bone, and cultured osteoblasts but not in cultured osteoclasts (Fig. 1 D). The expression in osteoblasts was finally confirmed by in situ hybridization

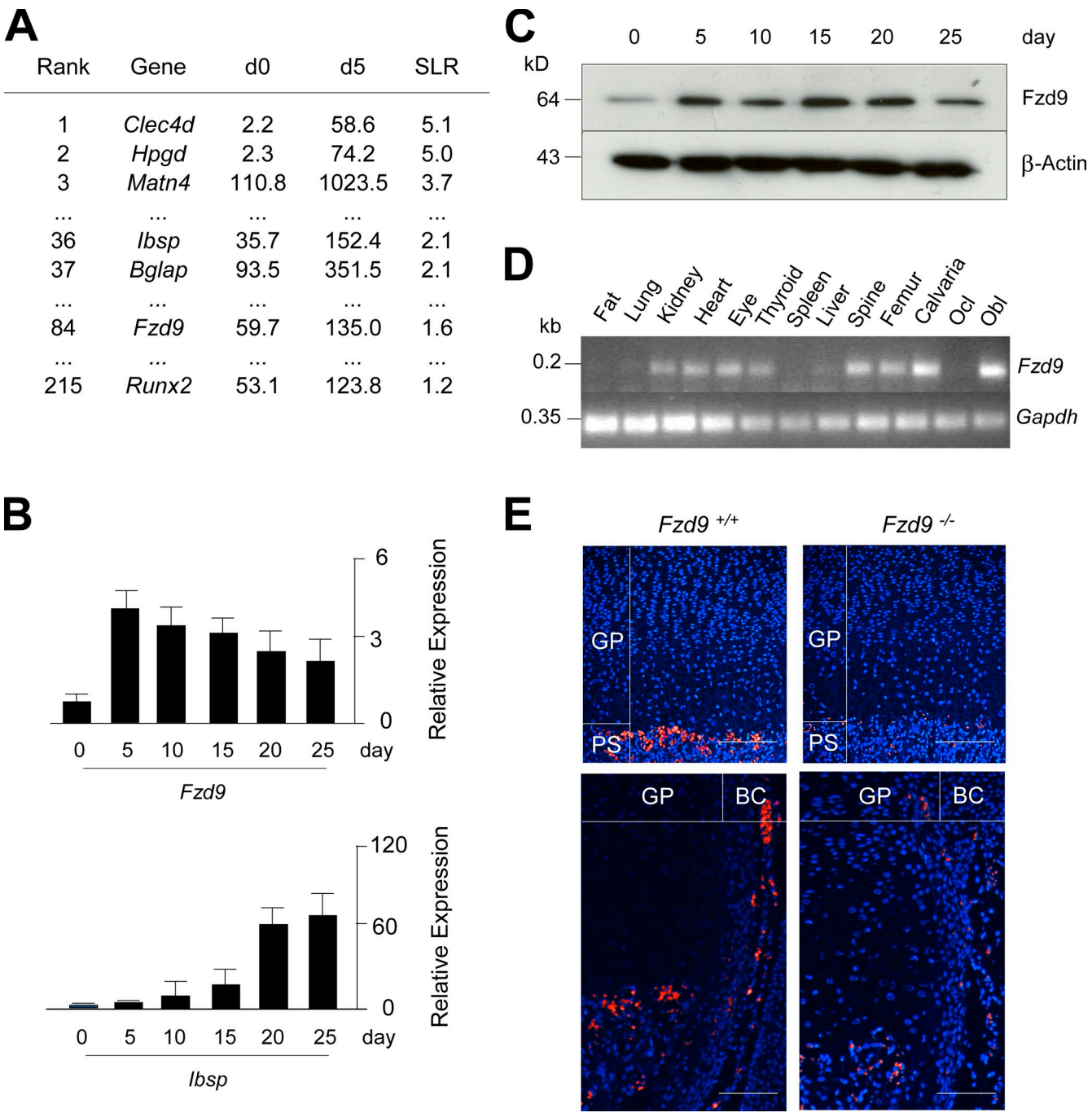

Figure 1. **Expression of *Fzd9* in osteoblasts.** (A) Ranking of the genes with the strongest induction of expression between day 0 (d0) and day 5 (d5) of primary osteoblast differentiation. Given are the signal intensities (Affymetrix) for both time points and the signal log ratios (SLR). (B) qRT-PCR for *Fzd9* and *Ibsp* expression between day 0 and day 25 of primary osteoblast differentiation. Error bars represent means ± SD (n = 3). (C) Western blot confirming the presence of Fzd9 in primary osteoblasts. (D) RT-PCR analysis of Fzd9 expression in various tissues and primary bone cells (Ocl, osteoclast; Obl, osteoblast). (E) In situ hybridization in tibia sections from 3-d-old wild-type (*Fzd9*$^{+/+}$) and *Fzd9*-deficient (*Fzd9*$^{-/-}$) mice showing *Fzd9* expression in the primary spongiosa (PS) and the bone collar (BC) region but not in the growth plate (GP). Bars, 200 µm. Black lines indicate that intervening lanes have been spliced out.

using tibiae from wild-type and *Fzd9*$^{-/-}$ mice, in which we found *Fzd9* transcripts only in the primary spongiosa and the bone collar region of wild-type sections (Fig. 1 E). Collectively, these findings led us to analyze the skeletal phenotype of *Fzd9*$^{-/-}$ mice, which have been described to display no major abnormalities besides a defect of B cell differentiation (Ranheim et al., 2005).

Fzd9-deficient mice display osteopenia caused by decreased bone formation

Because we did not observe defects of skeletal development in mice lacking *Fzd9*, we went on to perform nondecalcified histology of the spine at the ages of 6, 24, and 52 wk. Here, we found no significant difference between wild-type and *Fzd9*$^{-/-}$ littermates at 6 wk of age, but thereafter, bone mass was largely

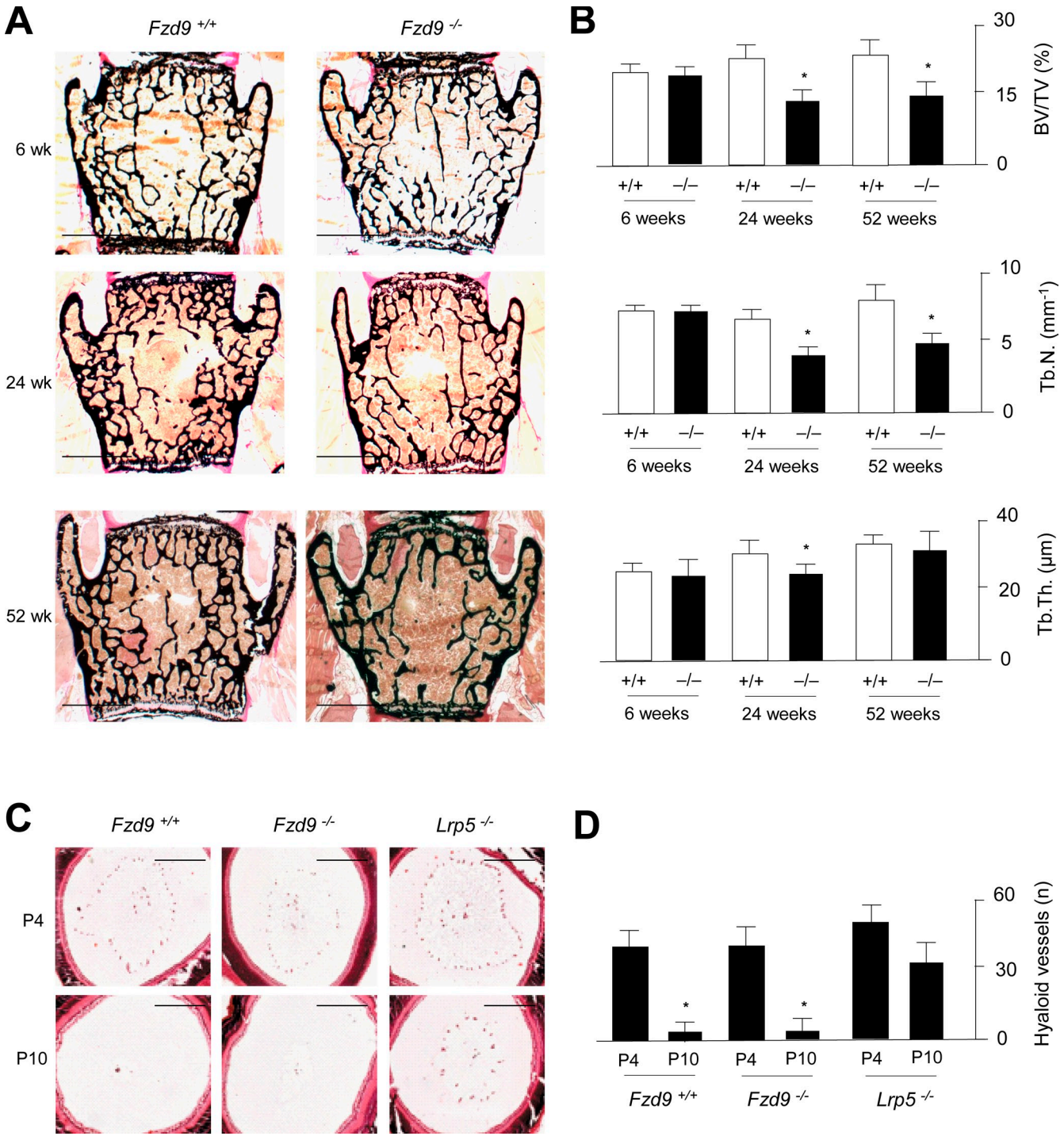

Figure 2. **Osteopenia in *Fzd9*-deficient mice.** (A) von Kossa/van Gieson staining of nondecalcified sections from vertebral bodies of wild-type and *Fzd9*$^{-/-}$ mice at the indicated ages. Bars, 1 mm. (B) Histomorphometric quantification of the trabecular bone volume per tissue volume (BV/TV), the trabecular number (Tb.N.), and the trabecular thickness (Tb.Th.) in wild-type (white bars) and *Fzd9*$^{-/-}$ (black bars) mice. (C) Hematoxylin/eosin staining of eyeballs from 4-d-old (P4) and 10-d-old (P10) wild-type, *Fzd9*$^{-/-}$, and *Lrp5*$^{-/-}$ mice. Bars, 250 µm. (D) Quantification of hyaloid vessels. All error bars represent means ± SD (n = 6). Asterisks indicate statistically significant differences ($P < 0.05$).

affected by the absence of *Fzd9* (Fig. 2 A). In fact, histomorphometric quantification of the trabecular bone volume revealed a reduction in *Fzd9*$^{-/-}$ vertebral bodies by 35 and 40% at the ages of 24 and 52 wk, respectively, which was mostly attributed to a lower trabecular number, whereas trabecular thickness was only moderately affected (Fig. 2 B). Because the deficiency of *Lrp5* also causes persistent embryonic eye vascularization, we next analyzed vascular regression in *Fzd9*$^{-/-}$ mice at day 4 and day 10 after birth (Fig. 2 C). Unlike the case in *Lrp5*-deficient mice, we did observe a postnatal decrease in the number of hyaloid vessels in *Fzd9*$^{-/-}$ animals, thereby ruling out an additional phenotype associated with the *Fzd9* inactivation (Fig. 2 D).

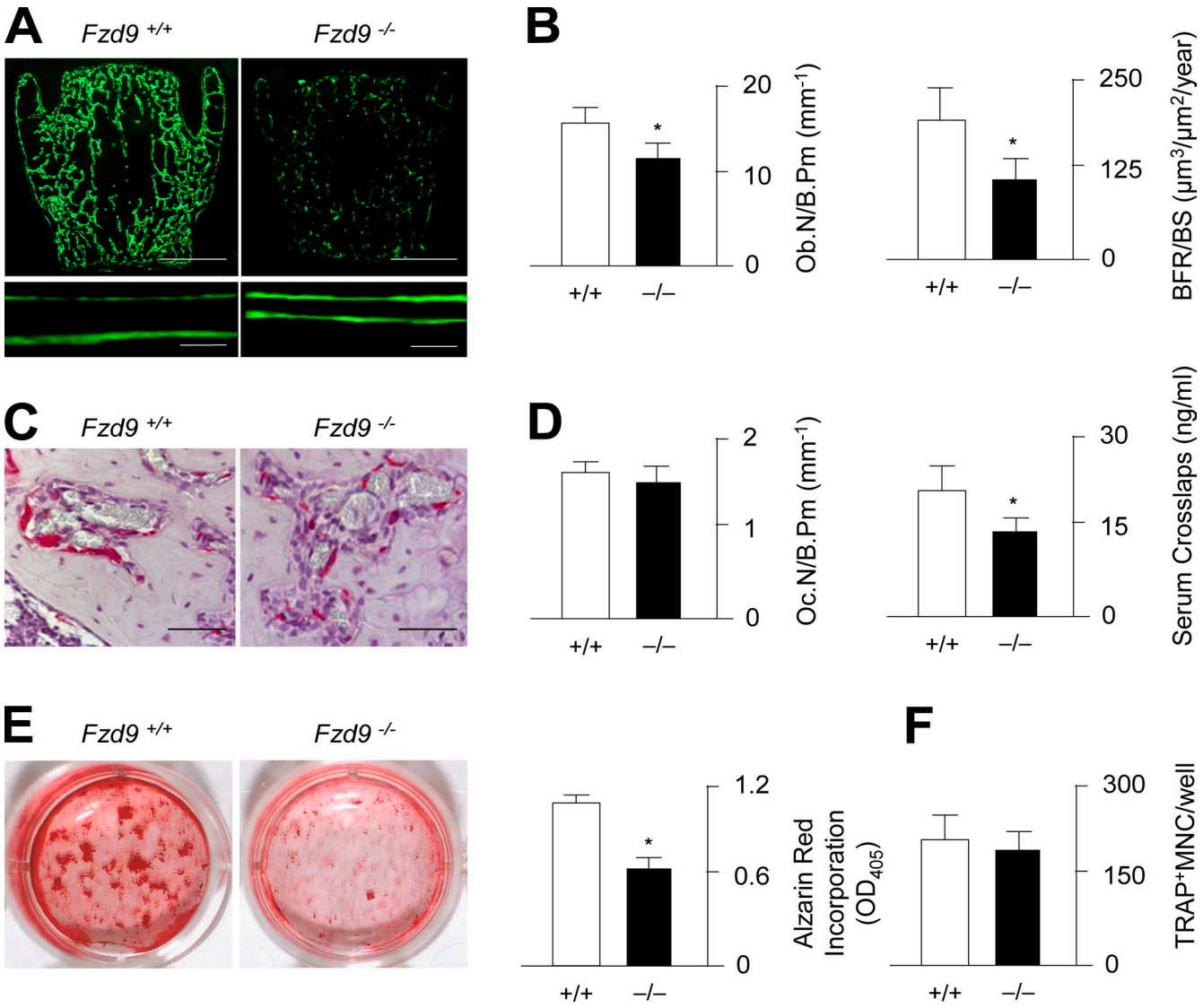

Figure 3. **Decreased bone formation rate in *Fzd9*-deficient mice.** (A) Fluorescent micrographs of vertebral body sections from 24-wk-old wild-type and *Fzd9*$^{-/-}$ mice reveal a reduced number of calcein-labeled surfaces and a smaller distance between labeling fronts in the latter ones. Bars: (top) 1 mm; (bottom) 20 µm. (B) Histomorphometric quantification of the osteoblast number per bone perimeter (Ob.N/B.Pm) and the bone formation rate per bone surface (BFR/BS). (C) TRAP activity staining of osteoclasts reveals no difference between 24-wk-old wild-type and *Fzd9*-deficient littermates. Bars, 50 µm. (D) Histomorphometric quantification of the osteoclast number per bone perimeter and concentrations of collagen degradation products (CrossLaps) in the serum. (B and D) $n = 6$. (E) Alizarin red staining of bone marrow cells differentiated into osteoblasts for 10 d and quantification of the mineralized area. (F) Quantification of the number of TRAP-positive multinucleated (MNC) osteoclasts differentiated from bone marrow precursor cells of wild-type and *Fzd9*$^{-/-}$ mice. (E and F) $n = 3$. Error bars represent means ± SD. Asterisks indicate statistically significant differences ($P < 0.05$).

To uncover the cellular basis of the osteopenia observed in *Fzd9*$^{-/-}$ mice, we next determined the histomorphometric parameters of bone formation and bone resorption. After dual injection of calcein, a fluorescent dye that binds to newly formed bone, we were able to demonstrate that bone formation was largely decreased in *Fzd9*$^{-/-}$ mice, as illustrated by a lower number of calcein-labeled surfaces but also by a reduced distance between the two labeling fronts at sites of double labeling (Fig. 3 A). Likewise, when we quantified the osteoblast number and bone formation rate, we observed a 30 and 45% reduction, respectively, in 24-wk-old *Fzd9*$^{-/-}$ mice (Fig. 3 B). In contrast, when we performed tartrate-resistant acid phosphatase (TRAP) activity staining of osteoclasts, we did not find a significant difference between wild-type and *Fzd9*$^{-/-}$ littermates (Fig. 3 C). This was subsequently confirmed by histomorphometry, in which we found no change in the numbers of osteoclasts per bone surface (Fig. 3 D). Thus, it appears that the significant reduction of bone-specific collagen degradation products found in the serum of *Fzd9*$^{-/-}$ mice is rather the consequence of their decreased bone volume.

To confirm the deduced hypothesis that the osteopenia of *Fzd9*$^{-/-}$ mice is primarily caused by a cell-autonomous defect of bone formation, we next isolated bone marrow stromal cells from wild-type and *Fzd9*$^{-/-}$ littermates and differentiated them by adding ascorbate and β-glycerophosphate. By performing alizarin red staining with subsequent quantification, we were able to demonstrate a decreased mineralization of *Fzd9*$^{-/-}$ cells ex vivo (Fig. 3 E). In contrast, when we differentiated bone marrow

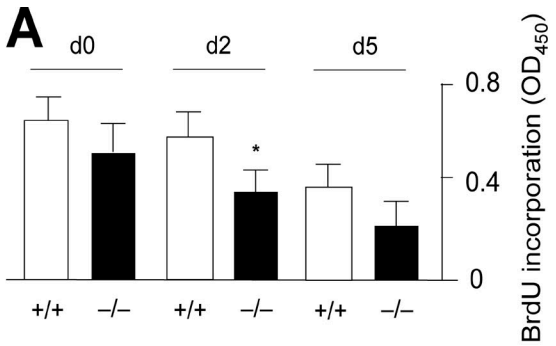

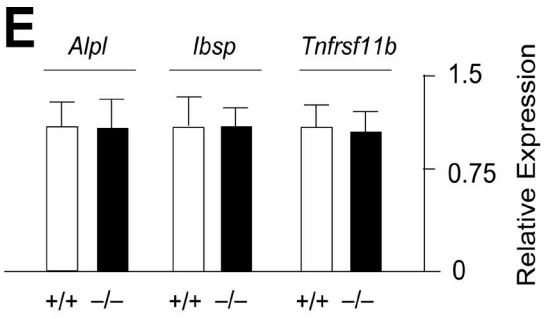

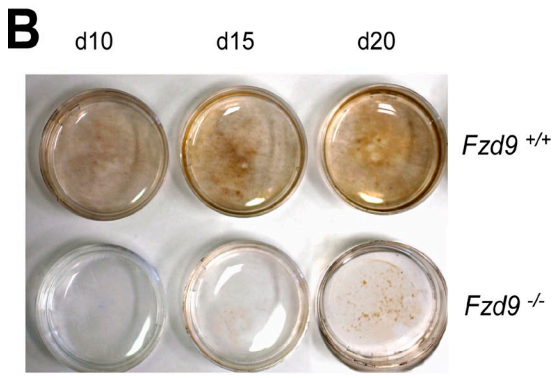

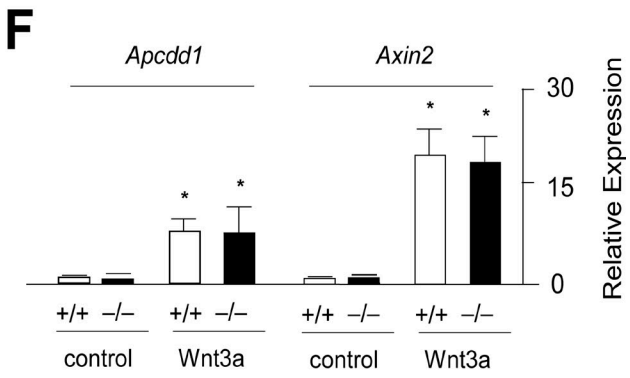

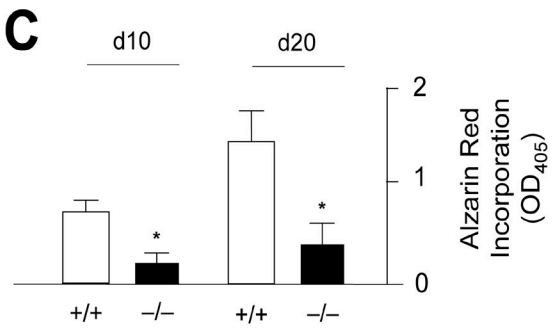

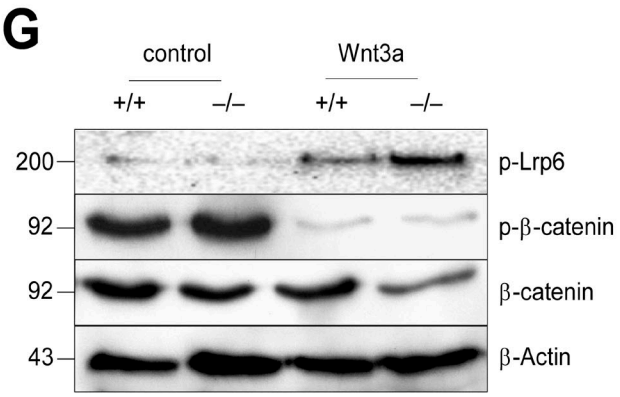

D

Gene	+/+	–/–	SLR
Runx2	57	46	-0.2
Sp7	519	404	-0.4
Atf4	1624	1649	-0.2
Col1a1	13153	13580	0
Alpl	842	1033	+0.3
Bglap	2524	1450	-0.7
Ibsp	2003	1716	-0.3
Dmp1	333	241	-0.2
Phex	85	78	0
Tnfrsf11b	1675	1650	-0.2
Axin2	109	82	-0.5
Apcdd1	150	179	+0.5

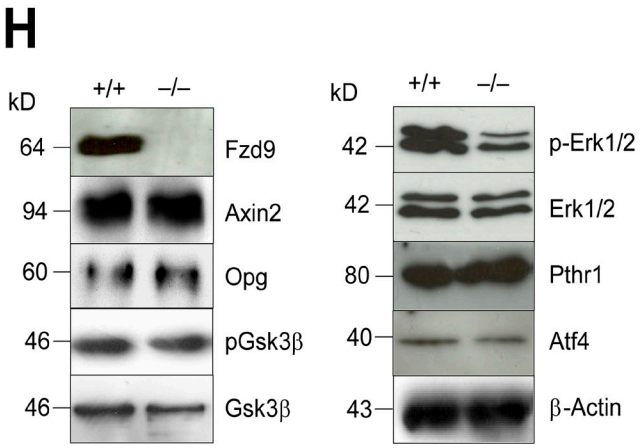

Figure 4. **Cell-autonomous defect of *Fzd9*-deficient osteoblasts.** (A) BrdU incorporation assay using wild-type and *Fzd9*$^{-/-}$ primary osteoblasts. $n = 8$. (B) von Kossa staining of the mineralized matrix reveals a cell-autonomous defect of bone formation in *Fzd9*$^{-/-}$ osteoblasts. (C) Quantification of the alizarin red incorporation in wild-type and *Fzd9*$^{-/-}$ primary osteoblasts at the indicated stages of differentiation. (D) Normal expression of known osteoblast

precursor cells into osteoclasts, there was no significant difference in the number of TRAP-positive multinucleated cells between wild-type and *Fzd9*$^{-/-}$ cultures (Fig. 3 F).

The cell-autonomous defect of *Fzd9*-deficient osteoblasts is not associated with impaired canonical Wnt signaling

Because bone marrow–derived osteoblast cultures contain a higher percentage of other cell types compared with calvaria-derived osteoblasts, we next isolated the primary cells from the calvariae of newborn mice to address the question of whether these *Fzd9*$^{-/-}$ cells would also display a cell-autonomous defect ex vivo. In the first set of experiments, we cultured the osteoblasts for 5 d in the presence of ascorbate and β-glycerophosphate and monitored their proliferation rate by BrdU incorporation assays. Here, we observed a transient decrease in *Fzd9*$^{-/-}$ cultures at day 2 of differentiation, thereby providing the first evidence for an intrinsic defect (Fig. 4 A). The second evidence came from a longer differentiation period, in which we analyzed the matrix mineralization of wild-type and *Fzd9*$^{-/-}$ osteoblasts after 10, 15, and 20 d of culturing using von Kossa staining (Fig. 4 B). Here, we found that *Fzd9*$^{-/-}$ cultures mineralized poorly until day 15 of differentiation and that the amount of mineralized matrix, again assessed by alizarin red staining, was largely decreased compared with wild-type cultures also after 20 d of differentiation (Fig. 4 C). To uncover the molecular basis of this cellular defect, we next isolated RNA from wild-type and *Fzd9*$^{-/-}$ cultures at day 10 of differentiation and subjected it to comparative GeneChip hybridization. Here, we first focused on the expression levels of several osteoblast differentiation markers, but we failed to detect differences between wild-type and *Fzd9*$^{-/-}$ cultures that were higher than twofold (Fig. 4 D). The same was the case for known target genes of the canonical Wnt signaling pathway, such as *Tnfrsf11b*, *Axin2*, and *Apcdd1* (Jho et al., 2002; Jukkola et al., 2004; Glass et al., 2005). To confirm these findings, we performed qRT-PCR using independently isolated cultures, in which we found no significant changes in the expression of *Alpl*, *Ibsp*, or *Tnfrsf11b* (Fig. 4 E).

To address the question of whether *Fzd9*$^{-/-}$ osteoblasts display a defect of canonical Wnt signaling, we next treated wild-type and *Fzd9*$^{-/-}$ cultures at day 10 of differentiation with recombinant Wnt3a for 6 h and thereafter monitored gene expression by qRT-PCR (Fig. 4 F). Here, we observed that the expression of the Wnt target genes *Axin2* and *Apcdd1* was induced to the same extent in wild-type and *Fzd9*$^{-/-}$ cells, thus demonstrating intact canonical Wnt signaling in the absence of Fzd9. This was also confirmed using Western blotting in which we observed that both the phosphorylation of Lrp6 and the reduced levels of phosphorylated β-catenin, induced by stimulation with Wnt3a, were not impaired by the absence of Fzd9 (Fig. 4 G).

We further performed a comparative Western blot analysis using untreated wild-type and *Fzd9*$^{-/-}$ osteoblasts at day 10 of differentiation. Here, we confirmed the normal expression of Axin2 and Opg, and we also detected no difference in the protein levels of Gsk3-β (Fig. 4 H). In contrast, we found decreased levels of phosphorylated Erk1/2 in *Fzd9*$^{-/-}$ cells, whereas there was no difference in the protein levels of the parathyroid hormone receptor or of ATF4, whose presence in osteoblasts is primarily controlled posttranslationally (Yang and Karsenty, 2004).

Decreased expression of chemokines and interferon-regulated genes in *Fzd9*-deficient osteoblasts

To further elucidate the molecular defects of *Fzd9*$^{-/-}$ osteoblasts, we next focused on the genes that displayed a more than twofold reduction of expression levels compared with wild-type cultures. Although none of these genes, at least at first sight, provided a reasonable explanation for the decreased bone formation caused by *Fzd9* deficiency, it was striking that there were two groups of genes whose expression appeared to be regulated by Fzd9, namely interferon-regulated genes and genes encoding chemokines (Fig. 5 A). To address the possible relevance of these findings, we first performed qRT-PCR for three members of both groups and observed a significantly reduced expression of *Oasl2*, *Isg15*, *Ifit1*, *Ccl5*, *Cxcl5*, and *Ccl2* in primary osteoblasts from *Fzd9*$^{-/-}$ mice (Fig. 5 B). To analyze whether this is also the case in vivo, we performed the same experiments with cDNA derived from femora of wild-type and *Fzd9*$^{-/-}$ mice and obtained similar results (Fig. 5 C).

Because the *Fzd9* deficiency did not impair canonical Wnt signaling, we next addressed the question of whether the genes with lower expression rates in *Fzd9*$^{-/-}$ osteoblasts were direct targets of Wnt5a, which is known to induce noncanonical signaling pathways. This was again assessed by qRT-PCR after a treatment of wild-type osteoblasts with either Wnt3a or Wnt5a for 6 h. Here, we found that Wnt5a did not stimulate the expression of *Axin2* and *Apccd1*, as expected, whereas it specifically induced the expression of the chemokine-encoding genes (Fig. 5 D). In contrast, there was no effect of either Wnt ligand on the expression of the interferon-regulated genes, whereas the expression of *Stat1*, encoding a key transcription factor in interferon-dependent signaling (Trinchieri, 2010), was induced by Wnt5a (Fig. 5 D). Because we further observed that Wnt5a induced Erk1/2 and Akt phosphorylation in wild-type osteoblasts, we next treated serum-starved wild-type and *Fzd9*$^{-/-}$ cells with Wnt5a for 30 min and then performed Western blotting to quantify the differences. Here, we found that the Wnt5a-induced phosphorylation of Erk1/2 and

differentiation markers and Wnt target genes in *Fzd9*$^{-/-}$ osteoblasts. Given are the signal intensities (Affymetrix) for wild-type and *Fzd9*$^{-/-}$ osteoblasts at day 10 (d10) of differentiation and the signal log ratios (SLR). (E) qRT-PCR expression analysis for the indicated genes in wild-type and *Fzd9*$^{-/-}$ osteoblasts. (F) qRT-PCR expression analysis for the indicated genes in wild-type and *Fzd9*$^{-/-}$ osteoblasts after a 6-h stimulation by Wnt3a. (C, E, and F) $n = 3$. (G) Western blotting with the indicated antibodies demonstrates that canonical Wnt signaling is unaffected in *Fzd9*$^{-/-}$ osteoblasts. Molecular mass markers represent kilodaltons. (H) Western blotting with the indicated antibodies demonstrates decreased Erk1/2 phosphorylation in *Fzd9*$^{-/-}$ osteoblasts. Error bars represent means ± SD. Asterisks indicate statistically significant differences ($P < 0.05$). Black lines indicate that intervening lanes have been spliced out.

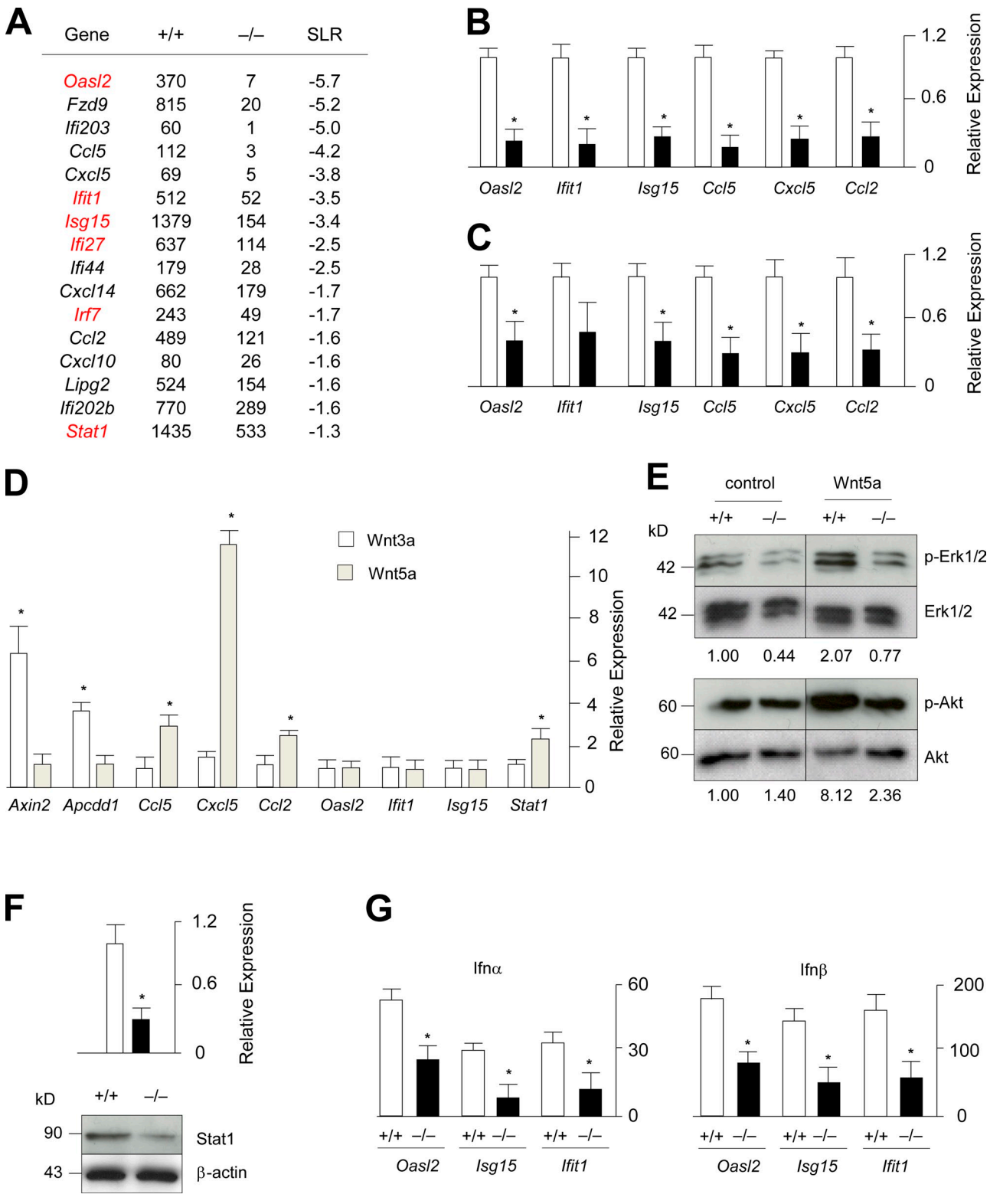

Figure 5. **Decreased expression of chemokines and interferon-regulated genes in *Fzd9*$^{-/-}$ osteoblasts.** (A) Signal intensities (Affymetrix) and signal log ratios for wild-type and *Fzd9*$^{-/-}$ osteoblasts at day 10 of differentiation. Besides *Fzd9* itself, genes either encode chemokines (*Cclx* and *Cxclx*) or have been identified as interferon regulated (*Oasl2*, *Ifix*, *Isg15*, *Ligp2*, and *Irfx*). Genes highlighted in red displayed a signal log ratio (SLR) >2.0 in the initial GeneChip experiment shown in Fig. 1 A. (B) qRT-PCR expression analysis for the indicated genes in wild-type and *Fzd9*$^{-/-}$ osteoblasts. (C) qRT-PCR expression analysis for the indicated genes in wild-type and *Fzd9*$^{-/-}$ femora. (D) qRT-PCR expression analysis for the indicated genes in wild-type osteoblasts treated for 6 h with Wnt3a or Wnt5a. (E) Western blotting with the indicated antibodies demonstrates decreased Erk1/2 and Akt phosphorylation in *Fzd9*$^{-/-}$ osteoblasts. The relative changes of the ratios between the phosphorylated and nonphosphorylated forms are given on the bottom. (F) qRT-PCR expression analysis and Western blotting demonstrate decreased *Stat1* expression in *Fzd9*$^{-/-}$ osteoblasts. (G) qRT-PCR expression analysis for the indicated genes in wild-type and *Fzd9*$^{-/-}$ osteoblasts after a 6-h stimulation by Ifn-α or Ifn-β. Error bars represent means ± SD (n = 3). Asterisks represent statistically significant differences ($P < 0.05$). Black lines indicate that intervening lanes have been spliced out.

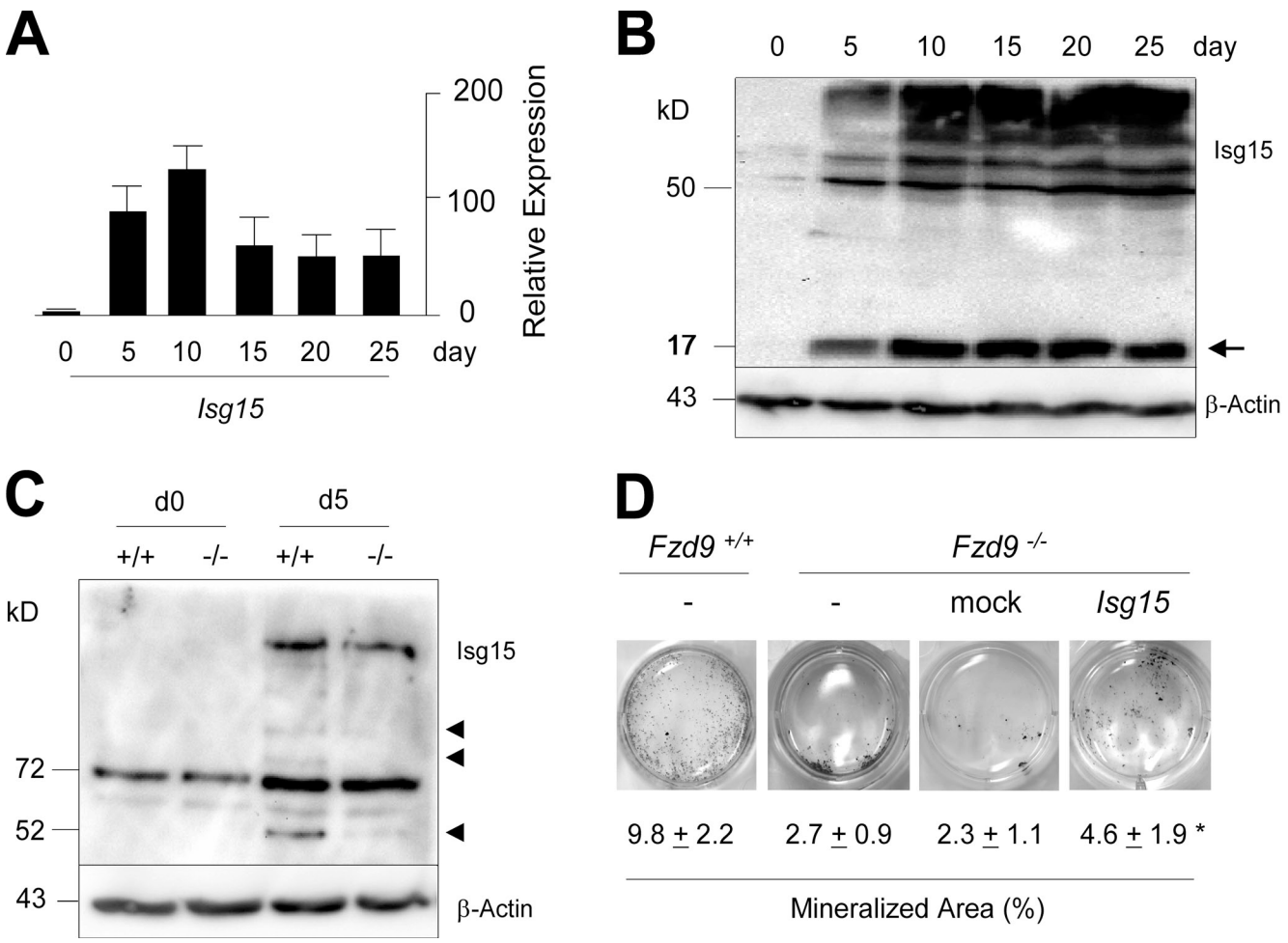

Figure 6. **Protein ISGylation in osteoblasts.** (A) qRT-PCR expression analysis for *Isg15* at different stages of primary osteoblast differentiation. Error bars represent means ± SD (n = 3). (B) Western blotting with an Isg15-specific antibody demonstrating an increase of free Isg15 (arrow) and ISGylated proteins during differentiation of wild-type osteoblasts. (C) Decreased ISGylation of specific proteins (arrowheads) in *Fzd9*$^{-/-}$ osteoblasts at day 5 (d5) of differentiation. (D) von Kossa staining of mineralized matrix in wild-type and *Fzd9*$^{-/-}$ osteoblasts at day 10 of differentiation. *Fzd9*$^{-/-}$ cultures were either transduced with an empty (mock) or an Isg15-encoding retroviral vector as indicated. Quantification of the mineralized area is given on the bottom. Values represent means ± SD (n = 3). The asterisk represents a statistically significant difference to untreated cells ($P < 0.05$). Black lines indicate that intervening lanes have been spliced out.

Akt was less pronounced in *Fzd9*$^{-/-}$ cells, thereby providing evidence for impaired noncanonical Wnt signaling in the absence of Fzd9 (Fig. 5 E).

Although we can only speculate so far on the relevance of the decreased chemokine expression in the absence of Fzd9, we followed up on the interferon-regulated genes because five of them (Fig. 5 A, highlighted in red) were found to display a signal log ratio >2.0 in our initial GeneChip hybridization comparing wild-type primary osteoblasts at day 0 and day 5 of differentiation. Because the same was the case for *Stat1*, we first confirmed its reduced expression in *Fzd9*$^{-/-}$ osteoblasts by qRT-PCR but also on the protein level using Western blotting (Fig. 5 F). To analyze whether the reduced levels of Stat1 in *Fzd9*$^{-/-}$ osteoblasts would impair interferon-dependent signaling, we next treated wild-type and *Fzd9*$^{-/-}$ osteoblasts with Ifn-α and Ifn-β for 6 h before we monitored gene expression by qRT-PCR. Here, we found that both ligands induced the expression of *Oasl2*, *Isg15*, and *Ifit1* in wild-type osteoblasts and that this effect was significantly reduced in *Fzd9*$^{-/-}$ cultures (Fig. 5 G).

The ubiquitin-like modifier Isg15 is involved in the regulation of bone formation

Given the striking defect of osteoblastogenesis caused by the absence of Fzd9, it would surely be interesting to analyze the role of each of its potential downstream regulators in future experiments. However, because *Isg15*, one of the interferon-regulated genes with decreased expression in *Fzd9*$^{-/-}$ osteoblasts, has recently gained a lot of attention, as it encodes a ubiquitin-like modifier protein (Loeb and Haas, 1992; Skaug and Chen, 2010), we went on to address the potential relevance of Isg15 in the regulation of bone formation. Using qRT-PCR, we first confirmed that *Isg15* expression levels increase during the early stages of osteoblast differentiation (Fig. 6 A). We then performed Western blotting using an Isg15-specific antibody and did not only observe an increase of free Isg15 during the differentiation process but also of ISGylated proteins (Fig. 6 B). In addition, we found that the ISGylation of specific proteins was less pronounced in *Fzd9*$^{-/-}$ cells at day 5 of differentiation (Fig. 6 C). We next addressed the question of whether the

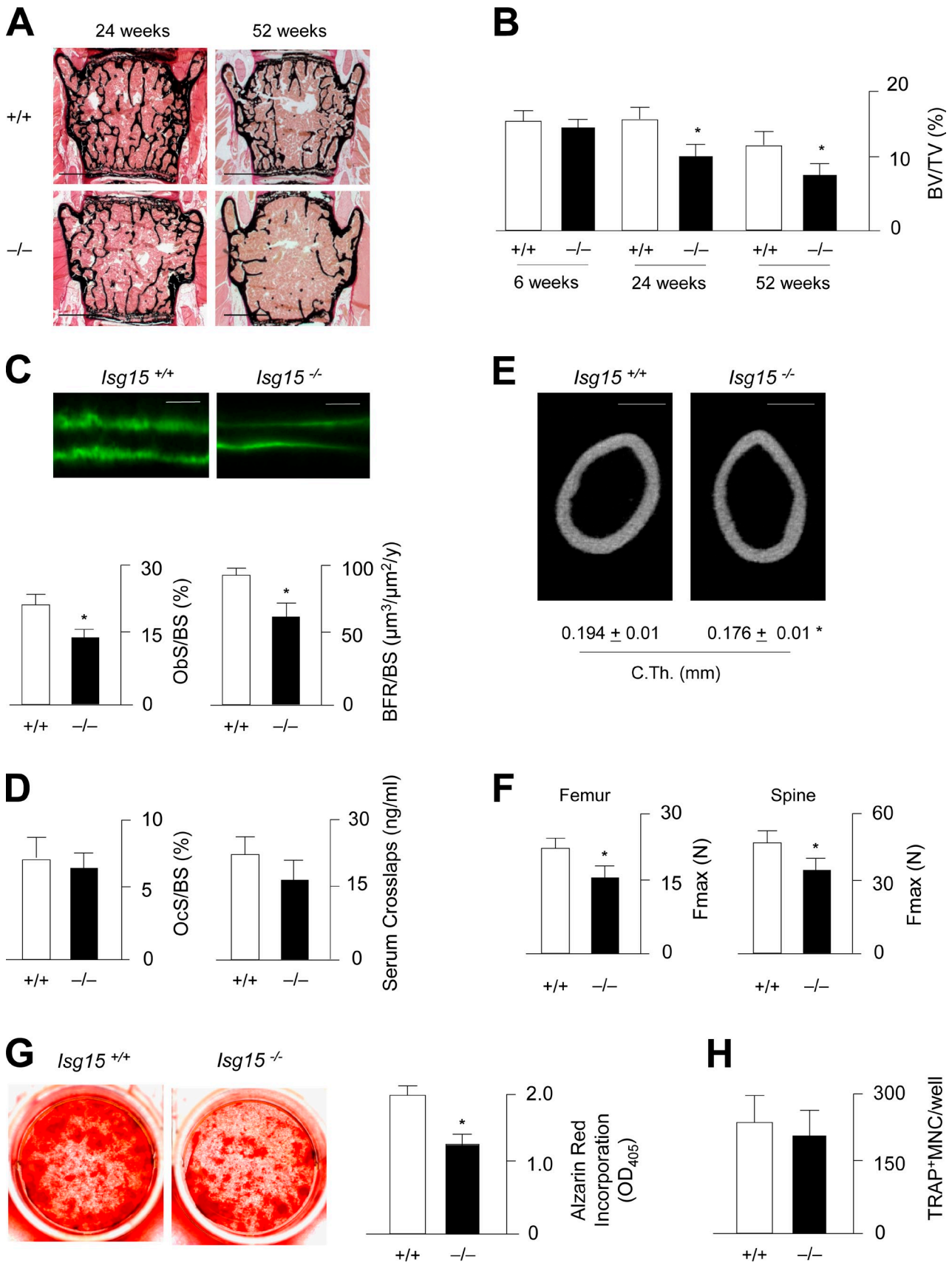

Figure 7. **Decreased bone formation in *Isg15*-deficient mice.** (A) von Kossa/van Gieson staining of nondecalcified sections of vertebral bodies from 24- and 52-wk-old wild-type and *Isg15*$^{-/-}$ mice. Bars, 1 mm. (B) Histomorphometric quantification of the trabecular bone volume at the indicated ages. BV/TV, bone volume per tissue volume. (C) Fluorescent micrographs reveal a reduced distance between the calcein-labeling fronts in 24-wk-old *Isg15*$^{-/-}$ mice.

restoration of *Isg15* expression in *Fzd9*$^{-/-}$ osteoblasts would rescue their defect of matrix mineralization. For that purpose, we transduced these cells at a nondifferentiated stage with an *Isg15*-expressing retrovirus and quantified the mineralized area at day 10 of differentiation. Here, we found a significant increase compared with mock-transfected cells, thus suggesting that Isg15 is one downstream effector of Fzd9 in osteoblasts (Fig. 6 D).

To analyze the role of Isg15 in bone remodeling in vivo, we took advantage of an *Isg15*-deficient mouse model, which has been described to display no obvious phenotype outside the skeleton (Osiak et al., 2005). Using nondecalcified histology of the spine (Fig. 7 A), we were able to demonstrate that the trabecular bone volume is significantly decreased in 24- and 52-wk-old *Isg15*$^{-/-}$ mice compared with wild-type littermates (Fig. 7 B). As is the case in *Fzd9*$^{-/-}$ mice, this phenotype is caused by decreased bone formation, which was assessed by cellular and dynamic histomorphometry (Fig. 7 C). In contrast, neither the number of osteoclasts nor their resorptive activity was affected by the absence of *Isg15* (Fig. 7 D). We further analyzed the cortical bone of the femora from wild-type and *Isg15*$^{-/-}$ mice and did not only observe a reduced cortical thickness in the latter ones (Fig. 7 E) but also a decreased biomechanical stability in three point–bending assays (Fig. 7 F). Likewise, the force until bone failure was reduced in *Isg15*$^{-/-}$ L6 vertebral bodies that were subjected to microcompression testing. Finally, we isolated bone marrow cells from wild-type and *Isg15*$^{-/-}$ mice and analyzed their ability to differentiate into osteoblasts and osteoclasts. Here, we obtained similar results as we did for *Fzd9*$^{-/-}$ cells, namely reduced mineralization after differentiation into osteoblasts (Fig. 7 G) but normal osteoclastogenesis (Fig. 7 H).

Low bone mass caused by *Fzd9* heterozygosity

Because *FZD9* is one of the genes whose hemizygous deletion in humans causes Williams–Beuren syndrome (WBS; Wang et al., 1997; Schubert, 2009) and because we have previously reported that individuals suffering from WBS display decreased bone mineral density (Cherniske et al., 2004), we finally addressed the question of whether *Fzd9*$^{+/-}$ mice would also display a low bone mass phenotype. For that purpose, we performed nondecalcified histology and microcomputed tomography (µCT) scanning of the spines from 70-wk-old wild-type, *Fzd9*$^{+/-}$, and *Fzd9*$^{-/-}$ mice and observed osteopenia in the two latter groups (Fig. 8 A). Likewise, using cross-sectional µCT scanning, we observed a reduced cortical thickness of *Fzd9*$^{+/-}$ and *Fzd9*$^{-/-}$ femora (Fig. 8 B). Histomorphometric quantification revealed that both *Fzd9*$^{+/-}$ and *Fzd9*$^{-/-}$ mice display a reduced trabecular bone volume, a lower number of osteoblasts, and a decreased bone formation rate compared with wild-type littermates (Fig. 8 C). Because one of the individuals with WBS had a history of three fractures within the thoracic and lumbar spine (Fig. 8 D), we further performed biomechanical testing of the mouse bones, in which we observed a decreased biomechanical competence of *Fzd9*$^{+/-}$ and *Fzd9*$^{-/-}$ vertebral bodies and femora (Fig. 8 E). Collectively, these latter findings underscore the relevance of Fzd9 for the regulation of bone remodeling in mice and raise the hypothesis that the osteopenia associated with WBS is explained, at least in part, by *FZD9* haploinsufficiency.

Discussion

FZD9 was first identified in 1997 and immediately gained a lot of attention because it is located on chromosome 7q11.23 within the region, whose hemizygous deletion causes WBS, a neurodevelopmental disorder associated with multiple additional manifestations (Wang et al., 1997; Schubert, 2009). To analyze the potential contribution of a *FZD9* deletion to the pathogenesis of WBS, the murine *Fzd9* gene was cloned 2 yr later and found expressed in a variety of tissues (Wang et al., 1999). The functional relevance of Fzd9 was subsequently analyzed through the generation of two different mouse deficiency models, both deleting the entire open reading frame (Ranheim et al., 2005; Zhao et al., 2005a). Not necessarily expected, *Fzd9*$^{-/-}$ mice developed normally, were fertile, and did not display any gross abnormalities. However, whereas one of the studies revealed hippocampal defects and learning deficits in *Fzd9*$^{-/-}$ mice (Zhao et al., 2005a), the other study did not detect obvious features of WBS in their mice, although they displayed abnormal B cell development (Ranheim et al., 2005). Because a skeletal analysis of both mouse models has not been reported elsewhere, the data presented in our manuscript provide the first evidence for a physiological role of Fzd9 as a regulator of bone formation. In addition, they are the first to demonstrate a functional role for one the Fzd family members in bone remodeling, which is important for our understanding of Wnt signaling in osteoblasts.

Given the fact that the bone formation phenotype of *Fzd9*$^{-/-}$ mice is caused by a cell-autonomous osteoblast defect, we were further able to analyze some of the molecular mechanisms underlying the observed phenotype. Here, we found that, although Fzd9 has previously been shown to activate β-catenin–dependent gene expression in 293T cells (Karasawa et al., 2002), canonical Wnt signaling was not impaired in *Fzd9*$^{-/-}$ osteoblasts, which is in full agreement with the absence of a bone formation phenotype in mice with altered β-catenin signaling in

Bars, 20 µm. The histomorphometric quantification of the osteoblast surface per bone surface (ObS/BS) and the bone formation rate is given on the bottom. (D) Histomorphometric quantification of the osteoclast surface per bone surface and concentrations of collagen degradation products in the serum. (E) Cross-sectional µCT scanning of the femora from of 24-wk-old wild-type and *Isg15*$^{-/-}$ mice. Bars, 500 µm. Quantifications of the cortical thickness (C.Th.) are given on the bottom. (F) Three point–bending assays of femora and microcompression testing of vertebral body L6 (spine) reveals that the force until bone failure (Fmax) is decreased in *Isg15*$^{-/-}$ mice. (B–D and F) $n = 6$. (G) Alizarin red staining of bone marrow cells differentiated into osteoblasts for 10 d and quantification of the mineralized area. (H) Quantification of the number of TRAP-positive multinucleated (MNC) osteoclasts differentiated from bone marrow precursor cells of wild-type and *Isg15*$^{-/-}$ mice. (G and H) $n = 3$. Error bars represent means ± SD. Asterisks indicate statistically significant differences ($P < 0.05$).

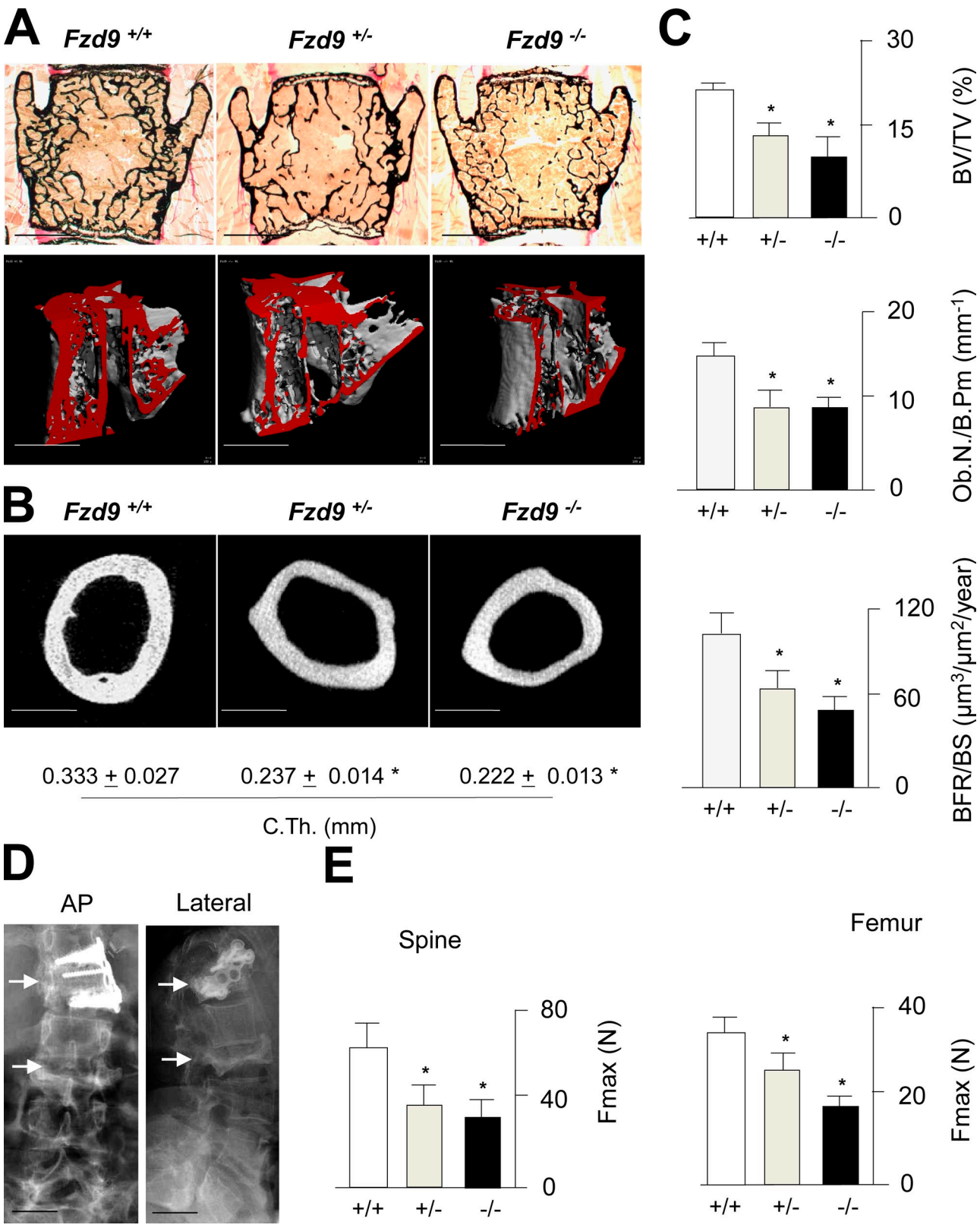

Figure 8. **Heterozygosity of *Fzd9* causes osteopenia.** (A) von Kossa/van Gieson staining of nondecalcified sections and µCT scanning of vertebral bodies from 70-wk-old wild-type, *Fzd9*$^{+/-}$, and *Fzd9*$^{-/-}$ mice. Bars, 1 mm. (B) Cross-sectional µCT scanning of femora. Bars, 500 µm. Quantifications of the cortical thickness (C.Th.) are given on the bottom. (C) Histomorphometric quantification of the trabecular bone volume, the osteoblast number, and the bone formation rate. BV/TV, bone volume per tissue volume; Ob.N/B.Pm, osteoblast number per bone perimeter; BFR/BS, bone formation rate per bone surface. (D) X rays of the spine from an individual with WBS and osteoporosis. Bars, 10 cm. Note the fractures of vertebral bodies (arrows), one of them being surgically stabilized. (E) Microcompression testing of the spine and three point–bending assays of femora demonstrate a decreased biomechanical stability of *Fzd9*$^{+/-}$ and *Fzd9*$^{-/-}$ bones. Fmax, force until bone failure. Error bars represent means ± SD (n = 6). Asterisks represent a statistically significant difference ($P < 0.05$).

osteoblasts (Glass et al., 2005; Holmen et al., 2005; Kramer et al., 2010). In fact, both the low bone mass phenotype of mice lacking β-catenin in osteoblasts and the osteopetrosis of mice expressing a stabilized form of β-catenin in osteoblasts are fully explained by impaired *Tnfrsf11b* expression, thereby triggering changes of osteoclast differentiation and bone resorption. Thus, because we neither observed decreased *Tnfrsf11b* expression nor increased bone resorption in *Fzd9*$^{-/-}$ mice, it appears that Fzd9 rather affects other signaling pathways. In addition, our findings further demonstrate that Fzd9 does not influence bone formation through an interaction with Lrp5 because *Lrp5*$^{-/-}$ osteoblasts do not display a cell-autonomous defect (Yadav et al., 2008) and because serotonin levels are normal in the serum of *Fzd9*$^{-/-}$ mice (unpublished data).

To understand the defect of *Fzd9*$^{-/-}$ osteoblasts at the molecular level, we further performed a comparative genome-wide expression analysis using GeneChip hybridization. Here, we did not observe striking differences in the expression of several well-established osteoblast differentiation markers and canonical Wnt-signaling target genes between wild-type and *Fzd9*-deficient cultures, but we did observe a reduced expression of chemokines and interferon-regulated genes in the latter ones. By treating wild-type osteoblasts with Wnt3a or Wnt5a, we were further able to demonstrate that the chemokine-encoding genes were direct targets of Wnt5a, which suggested that noncanonical Wnt signaling pathways could be impaired in *Fzd9*$^{-/-}$ osteoblasts. This was confirmed by Western blotting, in which we found that the known effects of Wnt5a on Erk1/2 and Akt phosphorylation (Almeida et al., 2005; Kawasaki et al., 2007; Peng et al., 2010) were essentially blunted in *Fzd9*$^{-/-}$ cells. Collectively, these results suggest that the presence of Fzd9 in osteoblasts is required to induce noncanonical Wnt signaling pathways, and they are in full agreement with the positive influence of increased Erk and Akt signaling on bone formation (Ford-Hutchinson et al., 2007; Ge et al., 2007). Whether an impaired expression of chemokines is involved in these effects remains to be established, and for now, we can only speculate about the possibility that their decreased expression in osteoblasts contributes to the low bone mass phenotype of *Fzd9*-deficient mice.

In contrast to the effect of Wnt5a on the expression of *Ccl5*, *Cxcl5*, and *Ccl2*, there was no direct influence of Wnt ligands on the expression of *Oasl2*, *Isg15*, and *Ifit1*. However, because Wnt5a did induce the expression of *Stat1*, it appears that the decreased expression of interferon-regulated genes in *Fzd9*$^{-/-}$ osteoblasts is the consequence of their reduced Stat1 protein levels. Consistent with this notion, we found that the expression of interferon-regulated genes is induced during the early differentiation stages of wild-type osteoblasts together with the expression of *Stat1* and *Fzd9*. In this paper, we have focused on one of these genes, *Isg15*, which appeared to be particularly interesting because it encodes a ubiquitin-like modifier protein and because the regulation of protein degradation has been demonstrated to be of critical importance for osteoblast activity (Yang and Karsenty, 2004; Jones et al., 2006). Triggered by the finding that protein ISGylation is reduced in *Fzd9*$^{-/-}$ osteoblasts, we embarked on the phenotypic analysis of *Isg15*$^{-/-}$ mice and observed osteopenia caused by decreased bone formation. In addition, we found that the cell-autonomous defect of *Fzd9*$^{-/-}$ osteoblasts is at least partially rescued after transduction of an Isg15 retrovirus, thus suggesting that Isg15 is one of the relevant downstream targets of Fzd9 in the regulation of bone formation. Although we could further demonstrate a cell-autonomous defect of osteoblast differentiation caused by *Isg15* deficiency, we were not yet able to identify the underlying mechanisms, which is best explained by the paucity of knowledge regarding the physiological role of Isg15 (Skaug and Chen, 2010).

Isg15 was identified as an interferon-induced gene with a molecular mass of 15 kD, which can be conjugated to target proteins in a three-step enzymatic cascade. Although this ISGylation process is similar to the conjugation of ubiquitin, Isg15 apparently does not influence proteasomal degradation but rather affects the function of its target proteins, similar to other posttranslational modifications (Okumura et al., 2007; Jeon et al., 2009; Shi et al., 2010). However, because proteomics studies have identified >300 potential target proteins and because recent evidence has suggested that Isg15 broadly targets newly synthesized proteins, it is difficult to address the question which of these ISGylated proteins are functionally relevant in osteoblasts (Zhao et al., 2005b; Durfee et al., 2010). In this regard, it is important to state that the observed osteopenia is the only spontaneously developing phenotype of *Isg15*$^{-/-}$ mice described so far. This implies that a thorough molecular comparison of wild-type and *Isg15*$^{-/-}$ osteoblasts could provide novel insights into the physiological role of Isg15, although this analysis is certainly beyond the scope of our manuscript.

Regardless of these open questions, we believe that the most relevant hypothesis raised by our study is that FZD9 might be involved in the regulation of bone formation in humans. To our knowledge, no *FZD9* mutations have been reported in individuals with bone loss disorders, yet it is tempting to speculate that the low bone mass in WBS individuals may be the consequence of their hemizygous deletion of the *FZD9* gene. To address this issue, we have performed dual x-ray energy absorptiometry in 15 individuals with WBS, aged between 30 and 50 yr, in which we found a mean T score below −1.0 in three different skeletal elements, which is indicative of osteopenia (unpublished data). Moreover, four of these individuals were diagnosed with osteoporosis (T score below −2.5), and one of them displayed fractures within the thoracic and lumbar spine. Although it is virtually impossible to prove that the reduced bone mineral density in WBS individuals is caused by FZD9 haploinsufficiency, there are at least two arguments derived from mouse experiments in favor of this hypothesis. First, among all the genes located in the WBS deletion region, *Fzd9* was the only one that is differentially expressed during primary osteoblast differentiation. Second, the loss of one *Fzd9* allele in mice resulted in osteopenia and reduced bone formation, and there were no statistically significant differences in our skeletal analysis between *Fzd9*$^{+/-}$ and *Fzd9*$^{-/-}$ mice at 70 wk of age.

Thus, based on these findings, we concur with our previous recommendation that bone densitometry should be routinely performed in individuals with WBS (Cherniske et al., 2004) because some percentage of them may benefit from one

of the currently available antiosteoporotic therapies. In addition, if future studies will provide further evidence for a role of FZD9 as a positive regulator of bone formation in humans, FZD9 itself could be considered as a target for osteoanabolic therapy. In fact, because FZD proteins are serpentine receptors, thus belonging to the major class of target proteins for currently available drugs (Wise et al., 2002; Overington et al., 2006), it might be possible to develop FZD9-specific agonists and to analyze them for bone anabolic activity. In this regard, it is again relevant that Fzd9 controls osteoblast function without affecting the canonical Wnt signaling pathway because recent evidence suggested that increased levels of β-catenin in osteoblasts cause a higher susceptibility to osteosarcoma development (Kansara et al., 2009).

Materials and methods

Cell culture

Primary osteoblasts were isolated from the calvariae of 5-d-old mice by sequential collagenase digestion as described previously (Schmidt et al., 2005). Differentiation was induced by the addition of 50 µg/ml ascorbate and 10 mM β-glycerophosphate. Total RNA was isolated using the TRIZOL reagent (Invitrogen) and further purified with the RNeasy Mini kit (QIAGEN). Proteins were isolated by cell lysis with radioimmunoprecipitation assay buffer (1% NP-40, 1% sodium desoxycholate, 0.1% sodium dodecylsulfate, 150 mM sodium chloride, 2 mM EDTA, and 10 mM sodium phosphate) containing a protease and phosphatase inhibitor cocktail (Roche). Proliferation rates were measured by BrdU incorporation assays using the Biotrak Cell Proliferation kit (GE Healthcare), and matrix mineralization was assessed using von Kossa staining or alizarin red staining as previously described (Eferl et al., 2004; Schmidt et al., 2005). To analyze the effects of Wnt and interferon ligands, cells were serum starved overnight and then stimulated for 30 min or 6 h by the addition of 100 ng/ml Wnt3a (1324-WN-002; R&D Systems), 100 ng/ml Wnt5a (645-WN-010; R&D Systems) 100 ng/ml Ifn-α (300-02A; PeproTech), or 100 ng/ml Ifn-β (300-02BC; PeproTech). Retroviral vector production and transductions for *Isg15* expression were performed essentially as previously described (Guerra et al., 2008). Bone marrow–derived osteoblasts and osteoclasts were generated and analyzed as described previously (Huebner et al., 2006).

Expression analysis

For the genome-wide expression analysis, 5 µg RNA was used for first-strand cDNA synthesis. Synthesis of biotinylated cRNA was performed using the IVT Labeling kit (Affymetrix). For GeneChip hybridization, the fragmented cRNA was incubated in hybridization solution at 45°C for 16 h before the GeneChips (U74v2A and MG-430 2.0; Affymetrix) were washed using the Fluidics Station 450 (Affymetrix). Microarrays were scanned with the GeneChip scanner (Scanner 7G; Affymetrix), and the signals were processed using GeneChip Operating Software (Affymetrix). Absolute and comparative analyses were performed using the Microarray Suite algorithm (Affymetrix). Annotations were further analyzed with interactive query analysis (Affymetrix). For RT-PCR expression analysis, 1 µg RNA was reversed transcribed using SuperScript III (Invitrogen) according to the manufacturer's instructions. Gene-specific primers were used to amplify *Fzd9*, 5′-AGTTTCCTCCTGACCGGTTT-3′ and 5′-GTGGCAGCAGTACATGGTTG-3′, and *Gapdh*, 5′-GACATCAAGAAGGTGGTGAAGCAG-3′ and 5′-CTCCTGTTATTATGGGGGTCTGG-3′. For in situ hybridization, the *Fzd9*-specific fragment was subcloned into pBluescript (Agilent Technologies) to generate [^{35}S]UTP-labeled riboprobes using the Riboprobe Combination System (Promega). qRT-PCR was performed using a StepOnePlus system (Applied Biosystems) and predesigned gene expression assays (TaqMan; Applied Biosystems) for *Fzd9*, *Ibsp*, *Alpl*, *Tnfrsf11b*, *Apcdd1*, *Axin2*, *Oasl2*, *Ifit1*, *Isg15*, *Ccl5*, *Cxcl5*, *Ccl2*, and *Stat1*. *Gapdh* and *B2m* expressions were used as internal controls. Relative quantification was performed according to the $\Delta\Delta C_T$ method.

Western blotting

For Western blotting, equal amounts of protein were subjected to SDS-PAGE and then transferred to polyvinylidene fluoride membranes (Hybond; GE Healthcare). Membranes were blocked for 1 h using blocking buffer (TBS containing 0.1% Tween 20 and 5% nonfat dry milk) and incubated with primary antibody at a dilution of 1:1,000 at 4°C overnight. The antibodies were directed against Fzd9 (AF2440; R&D Systems), β-actin (MAB1501; Millipore), phospho-Lrp6 (2568; Cell Signaling Technology), phospho–β-catenin (9561; Cell Signaling Technology), total β-catenin (9582; Cell Signaling Technology), axin-2 (ab32197; Abcam), Opg (AF459; R&D Systems), phospho–Gsk3-β (9336; Cell Signaling Technology), Gsk3-β (9315; Cell Signaling Technology), phospho-Erk1/2 (9101; Cell Signaling Technology), Erk1/2 (4695; Cell Signaling Technology), Pthr1 (05-517; Millipore), Atf4 (WH0000468M1; Sigma-Aldrich), p-Akt (4060; Cell Signaling Technology), Akt (9272; Cell Signaling Technology), Stat1 (9172; Cell Signaling Technology), and Isg15 (Osiak et al., 2005). Washing steps were performed with TBS containing 0.1% Tween 20. Secondary HRP-conjugated antibodies (Dako) were used at a dilution of 1:2,000. Image acquisition was performed using a photoscanner (Scanjet G4050; Hewlett-Packard). Quantification was performed using a gel documentation system (ChemiDoc XRS; Bio-Rad Laboratories).

Mice

Fzd9-deficient mice (129/Sv genetic background) and wild-type littermates were identified by PCR genotyping using primers amplifying the mutant, 5′-ATAGCCTGAAGAACGAGATCA-3′ and 5′-GCTTCCAGAGAAATGCCACA-3′, and wild-type, 5′-CAATACGGAGAAGCTGGAGA-3′ and 5′-CCCACCACCAAGGACATGAA-3′, alleles, respectively (Ranheim et al., 2005). *Isg15*-deficient mice (C57BL/6 genetic background) and wild-type littermates were identified by PCR genotyping using primers amplifying the mutant, 5′-CGCGAAGGGGCCAACCAAAGAA-3′ and 5′-AGCCCCGATGAGGATGAGGTGT-3′, and wild-type, 5′-GCCCCCATCCAGAGCCAGTGTT-3′ and 5′-AGCCCCGATGAGGATGAGGTGT-3′, alleles, respectively (Osiak et al., 2005). *Lrp5*-deficient mice (C57BL/6 genetic background) were obtained from The Jackson Laboratory (005823). To determine the bone formation rate, all mice received two calcein injections, 9 and 2 d before sacrifice. For the histological analysis of eyeballs, we performed hematoxylin/eosin staining of paraffin sections according to standard protocols.

Skeletal analysis

Before their skeletal analysis, all mice (genetic background C57BL/6) received two injections of calcein (9 and 2 d before sacrifice). After their initial analysis by contact x ray (Cabinet X-ray System; Faxitron X-ray Corporation), the vertebral bodies L2 to L5 and one tibia from each animal were dehydrated and embedded nondecalcified into methylmetacrylate for sectioning. Sections were either stained with toluidine blue or by the von Kossa/van Gieson procedure as previously described (Huebner et al., 2006). Static and cellular histomorphometry was performed on toluidine blue–stained sections using the OsteoMeasure system (Osteometrics) following the guidelines of the American Society of Bone and Mineral Research (Parfitt et al., 1987). Dynamic histomorphometry for the determination of the bone formation rate was performed on two consecutive nonstained 12-µm sections. TRAP activity staining was performed on decalcified sections using naphthol AS-MX phosphate (Sigma-Aldrich) and Fast Red Violet LB Salt (Sigma-Aldrich) in 40 mM acetate buffer, pH 5. All histological images were captured at room temperature using a microscope (Axio Scope; Carl Zeiss, Inc.) with a 1.25× (no medium; 0.035 NA), 20× (no medium; 0.045 NA), or 40× (no medium; 0.75 NA) objective fitted with a camera (AxioCam; Carl Zeiss, Inc.). Image acquisition was performed using Axiovision software (Carl Zeiss, Inc.). The cortical thickness of femora was quantified by µCT scanning using a µCT 40 (Scanco Medical). Biomechanical stability of the femora was determined by three point–bending assays, whereas maximum strength and overall stiffness of the vertebrae were determined by microcompression testing (Schinke et al., 2009). The rate of bone resorption was determined by measuring the amount of bone-specific collagen degradation products (CrossLaps) in the serum (AC-06F1; Immunodiagnostic Systems).

The authors would like to thank Olga Winter, Saskia Schlossarek, Gudrun Arndt, and Susanne Conrad for technical assistance.

This work was supported by grants from the Deutsche Forschungsgemeinschaft (SCHI 504/5-1 and SCHI 504/5-2) within the transregional research group Mechanisms of Fracture Healing and Bone Regeneration in Osteoporosis.

Submitted: 2 August 2010
Accepted: 16 February 2011

References

Almeida, M., L. Han, T. Bellido, S.C. Manolagas, and S. Kousteni. 2005. Wnt proteins prevent apoptosis of both uncommitted osteoblast progenitors and differentiated osteoblasts by beta-catenin-dependent and -independent signaling cascades involving Src/ERK and phosphatidylinositol 3-kinase/AKT. *J. Biol. Chem.* 280:41342–41351. doi:10.1074/jbc.M502168200

Bodine, P.V., W. Zhao, Y.P. Kharode, F.J. Bex, A.J. Lambert, M.B. Goad, T. Gaur, G.S. Stein, J.B. Lian, and B.S. Komm. 2004. The Wnt antagonist secreted frizzled-related protein-1 is a negative regulator of trabecular bone formation in adult mice. *Mol. Endocrinol.* 18:1222–1237. doi:10.1210/me.2003-0498

Boyden, L.M., J. Mao, J. Belsky, L. Mitzner, A. Farhi, M.A. Mitnick, D. Wu, K. Insogna, and R.P. Lifton. 2002. High bone density due to a mutation in LDL-receptor-related protein 5. *N. Engl. J. Med.* 346:1513–1521. doi:10.1056/NEJMoa013444

Cherniske, E.M., T.O. Carpenter, C. Klaiman, E. Young, J. Bregman, K. Insogna, R.T. Schultz, and B.R. Pober. 2004. Multisystem study of 20 older adults with Williams syndrome. *Am. J. Med. Genet. A.* 131A:255–264. doi:10.1002/ajmg.a.30400

Cummings, S.R., J. San Martin, M.R. McClung, E.S. Siris, R. Eastell, I.R. Reid, P. Delmas, H.B. Zoog, M. Austin, A. Wang, et al; FREEDOM Trial. 2009. Denosumab for prevention of fractures in postmenopausal women with osteoporosis. *N. Engl. J. Med.* 361:756–765. (published erratum appears in *N. Engl. J. Med*. 2009. 361: 1914) doi:10.1056/NEJMoa0809493

Day, T.F., X. Guo, L. Garrett-Beal, and Y. Yang. 2005. Wnt/beta-catenin signaling in mesenchymal progenitors controls osteoblast and chondrocyte differentiation during vertebrate skeletogenesis. *Dev. Cell*. 8:739–750. doi:10.1016/j.devcel.2005.03.016

Durfee, L.A., N. Lyon, K. Seo, and J.M. Huibregtse. 2010. The ISG15 conjugation system broadly targets newly synthesized proteins: implications for the antiviral function of ISG15. *Mol. Cell*. 38:722–732. doi:10.1016/j.molcel.2010.05.002

Eferl, R., A. Hoebertz, A.F. Schilling, M. Rath, F. Karreth, L. Kenner, M. Amling, and E.F. Wagner. 2004. The Fos-related antigen Fra-1 is an activator of bone matrix formation. *EMBO J.* 23:2789–2799. doi:10.1038/sj.emboj.7600282

Ford-Hutchinson, A.F., Z. Ali, S.E. Lines, B. Hallgrímsson, S.K. Boyd, and F.R. Jirik. 2007. Inactivation of Pten in osteo-chondroprogenitor cells leads to epiphyseal growth plate abnormalities and skeletal overgrowth. *J. Bone Miner. Res.* 22:1245–1259. doi:10.1359/jbmr.070420

Frost, M., T.E. Andersen, V. Yadav, K. Brixen, G. Karsenty, and M. Kassem. 2010. Patients with high-bone-mass phenotype owing to Lrp5-T253I mutation have low plasma levels of serotonin. *J. Bone Miner. Res.* 25:673–675. doi:10.1002/jbmr.44

Ge, C., G. Xiao, D. Jiang, and R.T. Franceschi. 2007. Critical role of the extracellular signal–regulated kinase–MAPK pathway in osteoblast differentiation and skeletal development. *J. Cell Biol.* 176:709–718. doi:10.1083/jcb.200610046

Glass, D.A. II, P. Bialek, J.D. Ahn, M. Starbuck, M.S. Patel, H. Clevers, M.M. Taketo, F. Long, A.P. McMahon, R.A. Lang, and G. Karsenty. 2005. Canonical Wnt signaling in differentiated osteoblasts controls osteoclast differentiation. *Dev. Cell*. 8:751–764. doi:10.1016/j.devcel.2005.02.017

Gong, Y., R.B. Slee, N. Fukai, G. Rawadi, S. Roman-Roman, A.M. Reginato, H. Wang, T. Cundy, F.H. Glorieux, D. Lev, et al; Osteoporosis-Pseudoglioma Syndrome Collaborative Group. 2001. LDL receptor-related protein 5 (LRP5) affects bone accrual and eye development. *Cell*. 107:513–523. doi:10.1016/S0092-8674(01)00571-2

Grundberg, E., E.M. Lau, M. Lorentzon, M. Karlsson, A. Holmberg, L. Groop, D. Mellström, E. Orwoll, H. Mallmin, C. Ohlsson, et al. 2008. Large-scale association study between two coding LRP5 gene polymorphisms and bone phenotypes and fractures in men. *Osteoporos. Int.* 19:829–837 (published erratum appears in *Osteoporos. Int*. 2008. 19:1647. doi:10.1007/s00198-007-0512-z

Guerra, S., A. Cáceres, K.P. Knobeloch, I. Horak, and M. Esteban. 2008. Vaccinia virus E3 protein prevents the antiviral action of ISG15. *PLoS Pathog.* 4:e1000096. doi:10.1371/journal.ppat.1000096

Harada, S., and G.A. Rodan. 2003. Control of osteoblast function and regulation of bone mass. *Nature*. 423:349–355. doi:10.1038/nature01660

Hill, T.P., D. Später, M.M. Taketo, W. Birchmeier, and C. Hartmann. 2005. Canonical Wnt/beta-catenin signaling prevents osteoblasts from differentiating into chondrocytes. *Dev. Cell*. 8:727–738. doi:10.1016/j.devcel.2005.02.013

Holmen, S.L., C.R. Zylstra, A. Mukherjee, R.E. Sigler, M.C. Faugere, M.L. Bouxsein, L. Deng, T.L. Clemens, and B.O. Williams. 2005. Essential role of beta-catenin in postnatal bone acquisition. *J. Biol. Chem.* 280:21162–21168. doi:10.1074/jbc.M501900200

Hu, H., M.J. Hilton, X. Tu, K. Yu, D.M. Ornitz, and F. Long. 2005. Sequential roles of Hedgehog and Wnt signaling in osteoblast development. *Development*. 132:49–60. doi:10.1242/dev.01564

Huebner, A.K., T. Schinke, M. Priemel, S. Schilling, A.F. Schilling, R.B. Emeson, J.M. Rueger, and M. Amling. 2006. Calcitonin deficiency in mice progressively results in high bone turnover. *J. Bone Miner. Res.* 21:1924–1934. doi:10.1359/jbmr.060820

Jeon, Y.J., J.S. Choi, J.Y. Lee, K.R. Yu, S.M. Kim, S.H. Ka, K.H. Oh, K.I. Kim, D.E. Zhang, O.S. Bang, and C.H. Chung. 2009. ISG15 modification of filamin B negatively regulates the type I interferon-induced JNK signalling pathway. *EMBO Rep.* 10:374–380. doi:10.1038/embor.2009.23

Jho, E.H., T. Zhang, C. Domon, C.K. Joo, J.N. Freund, and F. Costantini. 2002. Wnt/beta-catenin/Tcf signaling induces the transcription of Axin2, a negative regulator of the signaling pathway. *Mol. Cell. Biol.* 22:1172–1183. doi:10.1128/MCB.22.4.1172-1183.2002

Jones, D.C., M.N. Wein, M. Oukka, J.G. Hofstaetter, M.J. Glimcher, and L.H. Glimcher. 2006. Regulation of adult bone mass by the zinc finger adapter protein Schnurri-3. *Science*. 312:1223–1227. doi:10.1126/science.1126313

Jukkola, T., N. Sinjushina, and J. Partanen. 2004. Drapc1 expression during mouse embryonic development. *Gene Expr. Patterns*. 4:755–762. doi:10.1016/j.modgep.2004.03.006

Kansara, M., M. Tsang, L. Kodjabachian, N.A. Sims, M.K. Trivett, M. Ehrich, A. Dobrovic, J. Slavin, P.F. Choong, P.J. Simmons, et al. 2009. Wnt inhibitory factor 1 is epigenetically silenced in human osteosarcoma, and targeted disruption accelerates osteosarcomagenesis in mice. *J. Clin. Invest.* 119:837–851. doi:10.1172/JCI37175

Karasawa, T., H. Yokokura, J. Kitajewski, and P.J. Lombroso. 2002. Frizzled-9 is activated by Wnt-2 and functions in Wnt/beta-catenin signaling. *J. Biol. Chem.* 277:37479–37486. doi:10.1074/jbc.M205658200

Kato, M., M.S. Patel, R. Levasseur, I. Lobov, B.H. Chang, D.A. Glass II, C. Hartmann, L. Li, T.H. Hwang, C.F. Brayton, et al. 2002. *Cbfa1*-independent decrease in osteoblast proliferation, osteopenia, and persistent embryonic eye vascularization in mice deficient in Lrp5, a Wnt coreceptor. *J. Cell Biol.* 157:303–314. doi:10.1083/jcb.200201089

Kawasaki, A., K. Torii, Y. Yamashita, K. Nishizawa, K. Kanekura, M. Katada, M. Ito, I. Nishimoto, K. Terashita, S. Aiso, and M. Matsuoka. 2007. Wnt5a promotes adhesion of human dermal fibroblasts by triggering a phosphatidylinositol-3 kinase/Akt signal. *Cell. Signal.* 19:2498–2506. doi:10.1016/j.cellsig.2007.07.023

Kramer, I., C. Halleux, H. Keller, M. Pegurri, J.H. Gooi, P.B. Weber, J.Q. Feng, L.F. Bonewald, and M. Kneissel. 2010. Osteocyte Wnt/beta-catenin signaling is required for normal bone homeostasis. *Mol. Cell. Biol.* 30:3071–3085. doi:10.1128/MCB.01428-09

Kubota, T., T. Michigami, N. Sakaguchi, C. Kokubu, A. Suzuki, N. Namba, N. Sakai, S. Nakajima, K. Imai, and K. Ozono. 2008. Lrp6 hypomorphic mutation affects bone mass through bone resorption in mice and impairs interaction with Mesd. *J. Bone Miner. Res.* 23:1661–1671. doi:10.1359/jbmr.080512

Li, J., I. Sarosi, R.C. Cattley, J. Pretorius, F. Asuncion, M. Grisanti, S. Morony, S. Adamu, Z. Geng, W. Qiu, et al. 2006. Dkk1-mediated inhibition of Wnt signaling in bone results in osteopenia. *Bone*. 39:754–766. doi:10.1016/j.bone.2006.03.017

Liberman, U.A. 2006. Long-term safety of bisphosphonate therapy for osteoporosis: a review of the evidence. *Drugs Aging*. 23:289–298. doi:10.2165/00002512-200623040-00002

Little, R.D., J.P. Carulli, R.G. Del Mastro, J. Dupuis, M. Osborne, C. Folz, S.P. Manning, P.M. Swain, S.C. Zhao, B. Eustace, et al. 2002. A mutation in the LDL receptor-related protein 5 gene results in the autosomal dominant high-bone-mass trait. *Am. J. Hum. Genet.* 70:11–19. doi:10.1086/338450

Loeb, K.R., and A.L. Haas. 1992. The interferon-inducible 15-kDa ubiquitin homolog conjugates to intracellular proteins. *J. Biol. Chem.* 267:7806–7813.

Mao, J., J. Wang, B. Liu, W. Pan, G.H. Farr III, C. Flynn, H. Yuan, S. Takada, D. Kimelman, L. Li, and D. Wu. 2001. Low-density lipoprotein receptor-related protein-5 binds to Axin and regulates the canonical Wnt signaling pathway. *Mol. Cell*. 7:801–809. doi:10.1016/S1097-2765(01)00224-6

Morvan, F., K. Boulukos, P. Clément-Lacroix, S. Roman Roman, I. Suc-Royer, B. Vayssière, P. Ammann, P. Martin, S. Pinho, P. Pognonec, et al. 2006. Deletion of a single allele of the Dkk1 gene leads to an increase in bone formation and bone mass. *J. Bone Miner. Res.* 21:934–945. doi:10.1359/jbmr.060311

Okumura, F., W. Zou, and D.E. Zhang. 2007. ISG15 modification of the eIF4E cognate 4EHP enhances cap structure-binding activity of 4EHP. *Genes Dev.* 21:255–260. doi:10.1101/gad.1521607

Osiak, A., O. Utermöhlen, S. Niendorf, I. Horak, and K.P. Knobeloch. 2005. ISG15, an interferon-stimulated ubiquitin-like protein, is not essential

for STAT1 signaling and responses against vesicular stomatitis and lymphocytic choriomeningitis virus. *Mol. Cell. Biol.* 25:6338–6345. doi:10.1128/MCB.25.15.6338-6345.2005

Overington, J.P., B. Al-Lazikani, and A.L. Hopkins. 2006. How many drug targets are there? *Nat. Rev. Drug Discov.* 5:993–996. doi:10.1038/nrd2199

Parfitt, A.M., M.K. Drezner, F.H. Glorieux, J.A. Kanis, H. Malluche, P.J. Meunier, S.M. Ott, and R.R. Recker. 1987. Bone histomorphometry: standardization of nomenclature, symbols, and units. Report of the ASBMR Histomorphometry Nomenclature Committee. *J. Bone Miner. Res.* 2:595–610. doi:10.1002/jbmr.5650020617

Peng, L., G. Dong, P. Xu, L.B. Ren, C.L. Wang, M. Aragon, X.D. Zhou, and L. Ye. 2010. Expression of Wnt5a in tooth germs and the related signal transduction analysis. *Arch. Oral Biol.* 55:108–114. doi:10.1016/j.archoralbio.2009.12.002

Ramirez Rodriguez, S.P., D.H. Morton, S.A. Garcia Merino, and E.A. Streeten. 2010. Elevated serum serotonin levels in patients with osteoporosis-pseudoglioma syndrome. *Endocr. Rev.* 31:S1900.

Ranheim, E.A., H.C.K. Kwan, T. Reya, Y.K. Wang, I.L. Weissman, and U. Francke. 2005. Frizzled 9 knock-out mice have abnormal B-cell development. *Blood*. 105:2487–2494. doi:10.1182/blood-2004-06-2334

Richards, J.B., F. Rivadeneira, M. Inouye, T.M. Pastinen, N. Soranzo, S.G. Wilson, T. Andrew, M. Falchi, R. Gwilliam, K.R. Ahmadi, et al. 2008. Bone mineral density, osteoporosis, and osteoporotic fractures: a genome-wide association study. *Lancet*. 371:1505–1512. doi:10.1016/S0140-6736(08)60599-1

Rodan, G.A., and T.J. Martin. 2000. Therapeutic approaches to bone diseases. *Science*. 289:1508–1514. doi:10.1126/science.289.5484.1508

Saarinen, A., T. Saukkonen, T. Kivelä, U. Lahtinen, C. Laine, M. Somer, S. Toiviainen-Salo, W.G. Cole, A.E. Lehesjoki, and O. Mäkitie. 2010. Low density lipoprotein receptor-related protein 5 (LRP5) mutations and osteoporosis, impaired glucose metabolism and hypercholesterolaemia. *Clin. Endocrinol. (Oxf.)*. 72:481–488. doi:10.1111/j.1365-2265.2009.03680.x

Sambrook, P., and C. Cooper. 2006. Osteoporosis. *Lancet*. 367:2010–2018. doi:10.1016/S0140-6736(06)68891-0

Schinke, T., A.F. Schilling, A. Baranowsky, S. Seitz, R.P. Marshall, T. Linn, M. Blaeker, A.K. Huebner, A. Schulz, R. Simon, et al. 2009. Impaired gastric acidification negatively affects calcium homeostasis and bone mass. *Nat. Med.* 15:674–681. doi:10.1038/nm.1963

Schmidt, K., T. Schinke, M. Haberland, M. Priemel, A.F. Schilling, C. Mueldner, J.M. Rueger, E. Sock, M. Wegner, and M. Amling. 2005. The high mobility group transcription factor Sox8 is a negative regulator of osteoblast differentiation. *J. Cell Biol.* 168:899–910. doi:10.1083/jcb.200408013

Schubert, C. 2009. The genomic basis of the Williams-Beuren syndrome. *Cell. Mol. Life Sci.* 66:1178–1197. doi:10.1007/s00018-008-8401-y

Schulte, G., and V. Bryja. 2007. The Frizzled family of unconventional G-protein-coupled receptors. *Trends Pharmacol. Sci.* 28:518–525. doi:10.1016/j.tips.2007.09.001

Schulze, J., S. Seitz, H. Saito, M. Schneebauer, R.P. Marshall, A. Baranowsky, B. Busse, A.F. Schilling, F.W. Friedrich, J. Albers, et al. 2010. Negative regulation of bone formation by the transmembrane Wnt antagonist Kremen-2. *PLoS ONE*. 5:e10309. doi:10.1371/journal.pone.0010309

Shi, H.X., K. Yang, X. Liu, X.Y. Liu, B. Wei, Y.F. Shan, L.H. Zhu, and C. Wang. 2010. Positive regulation of interferon regulatory factor 3 activation by Herc5 via ISG15 modification. *Mol. Cell. Biol.* 30:2424–2436. doi:10.1128/MCB.01466-09

Sims, A.M., N. Shephard, K. Carter, T. Doan, A. Dowling, E.L. Duncan, J. Eisman, G. Jones, G. Nicholson, R. Prince, et al. 2008. Genetic analyses in a sample of individuals with high or low BMD shows association with multiple Wnt pathway genes. *J. Bone Miner. Res.* 23:499–506. doi:10.1359/jbmr.071113

Skaug, B., and Z.J. Chen. 2010. Emerging role of ISG15 in antiviral immunity. *Cell*. 143:187–190. doi:10.1016/j.cell.2010.09.033

Teitelbaum, S.L., and F.P. Ross. 2003. Genetic regulation of osteoclast development and function. *Nat. Rev. Genet.* 4:638–649. doi:10.1038/nrg1122

Trinchieri, G. 2010. Type I interferon: friend or foe? *J. Exp. Med.* 207:2053–2063. doi:10.1084/jem.20101664

van Meurs, J.B., T.A. Trikalinos, S.H. Ralston, S. Balcells, M.L. Brandi, K. Brixen, D.P. Kiel, B.L. Langdahl, P. Lips, O. Ljunggren, et al; GENOMOS Study. 2008. Large-scale analysis of association between LRP5 and LRP6 variants and osteoporosis. *JAMA*. 299:1277–1290. doi:10.1001/jama.299.11.1277

Wang, Y.K., C.H. Samos, R. Peoples, L.A. Pérez-Jurado, R. Nusse, and U. Francke. 1997. A novel human homologue of the *Drosophila* frizzled wnt receptor gene binds wingless protein and is in the Williams syndrome deletion at 7q11.23. *Hum. Mol. Genet.* 6:465–472. doi:10.1093/hmg/6.3.465

Wang, Y.K., R. Spörle, T. Paperna, K. Schughart, and U. Francke. 1999. Characterization and expression pattern of the frizzled gene Fzd9, the mouse homolog of FZD9 which is deleted in Williams-Beuren syndrome. *Genomics*. 57:235–248. doi:10.1006/geno.1999.5773

Wehrli, M., S.T. Dougan, K. Caldwell, L. O'Keefe, S. Schwartz, D. Vaizel-Ohayon, E. Schejter, A. Tomlinson, and S. DiNardo. 2000. arrow encodes an LDL-receptor-related protein essential for Wingless signalling. *Nature*. 407:527–530. doi:10.1038/35035110

Wise, A., K. Gearing, and S. Rees. 2002. Target validation of G-protein coupled receptors. *Drug Discov. Today*. 7:235–246. doi:10.1016/S1359-6446(01)02131-6

Wodarz, A., and R. Nusse. 1998. Mechanisms of Wnt signaling in development. *Annu. Rev. Cell Dev. Biol.* 14:59–88. doi:10.1146/annurev.cellbio.14.1.59

Yadav, V.K., J.H. Ryu, N. Suda, K.F. Tanaka, J.A. Gingrich, G. Schütz, F.H. Glorieux, C.Y. Chiang, J.D. Zajac, K.L. Insogna, et al. 2008. Lrp5 controls bone formation by inhibiting serotonin synthesis in the duodenum. *Cell*. 135:825–837. doi:10.1016/j.cell.2008.09.059

Yang, X., and G. Karsenty. 2004. ATF4, the osteoblast accumulation of which is determined post-translationally, can induce osteoblast-specific gene expression in non-osteoblastic cells. *J. Biol. Chem.* 279:47109–47114. doi:10.1074/jbc.M410010200

Zaidi, M. 2007. Skeletal remodeling in health and disease. *Nat. Med.* 13:791–801. doi:10.1038/nm1593

Zhao, C., C. Avilés, R.A. Abel, C.R. Almli, P. McQuillen, and S.J. Pleasure. 2005a. Hippocampal and visuospatial learning defects in mice with a deletion of frizzled 9, a gene in the Williams syndrome deletion interval. *Development*. 132:2917–2927. doi:10.1242/dev.01871

Zhao, C., C. Denison, J.M. Huibregtse, S. Gygi, and R.M. Krug. 2005b. Human ISG15 conjugation targets both IFN-induced and constitutively expressed proteins functioning in diverse cellular pathways. *Proc. Natl. Acad. Sci. USA*. 102:10200–10205. doi:10.1073/pnas.0504754102